Electrocatalysis at Single Nanoparticles

Kleijn, S.E.F.

2

Electrochemistry of Nanoparticles

Metal nanoparticles (NPs) find widespread application as a result of their unique physical and chemical properties. Among many applications, NPs have generated considerable interest in catalysis and electrocatalysis, where they provide a high surface area to mass ratio, and can be tailored to promote particular reaction pathways. The activity of NPs can be analyzed especially well using electrochemistry, which probes interfacial chemistry directly. In this review, we discuss key issues related to the electrochemistry of NPs. We highlight model studies that demonstrate exceptional control of NP shape and size, or mass transport conditions, that can provide key insights into the behavior of ensembles of NPs. Particular focus is on the challenge of ultimately measuring reactions at individual NPs, and relating the response to NP structure, which is leading to imaginative experiments that impact electrochemistry generally as well as broader surface and colloid science.

2.1 Introduction

Metal nanoparticles (NPs) have received a great deal of attention owing to their fascinating physical and chemical properties which can differ significantly from those of the bulk material. Interesting aspects of NPs include size- and shape-dependent interatomic bond distances,[1, 2] melting points,[1, 3] chemical reactivity,[4–6] and optical and electronic properties.[1, 7, 8] Furthermore, the small size of NPs has allowed nanoscale electrochemical processes to be probed, such as electric double layer effects on interfacial electron transfer reactions.[9–12] NPs find many technical applications, such as in catalysis,[5, 13, 14] sensors,[15–17] and spectroscopy (such as surface enhanced Raman spectroscopy),[17–19] as optical filters,[20] and in biomedical applications.[21–23]

Based on the application in hand, NPs are selected to achieve a particular function, from properties that emerge from both the constituent materials of the NP and its size. Significant research effort has thus aimed for a definitive understanding of shape and size effects on NP properties. In this context, electrochemical techniques are especially interesting, particularly when electrochemical characteristics can be related directly to other properties of the NP. The challenge of ultimately measuring the electrochemical behavior of individual NPs is leading to imaginative experiments that impact electrochemistry generally, as well as broader surface and colloid science, as we highlight in this chapter.

One of the largest applications of NPs is in electrocatalysis, the field of catalysis concerned with reactions that involve charge transfer at the interface between a solid catalyst and an electrolyte.[13] This area is key to the development of fuel cells and batteries, electrolyzers and electrosynthesic methods, as well as electrochemical sensing systems. The commercial viability of such devices requires the optimization of catalyst materials, not only to promote efficient use, but also to enhance selectivity towards a particular pathway.

The reduction of particle size to decrease catalyst cost and improve usage does not necessarily lead to an optimal catalytic performance, as catalytic activity does not always scale linearly with the NP surface area. Ultrasmall NPs may become nonmetal-like[24] and be more prone to poisoning,[25] and reaction pathways may depend strongly on NP size.[26] This is because the interaction energies between reactant molecules and metal surface atoms depend strongly on the local arrangement of the metal atoms in the surface, as evident in model (single-crystal) experiments[5, 27] and computational studies.[28] Moreover, the mass transport rates of reactants, products and

intermediates depend significantly on NP size and coverage on an electrode support. This makes the investigation of NP electrochemistry and electrocatalysis non-trivial, and, without proper controls may lead to ambiguities when comparing data from different types of experiments, as we discuss herein (Section 2.3).

In fuel cell applications, metal NP catalysts are supported on conductive carbon substrates and employed in membrane-electrode assemblies (MEAs; Fig 2.1a). These real catalysts have been studied in model environments to evaluate their performance as a function of composition (Fig 2.1b).[29] However, fuel cell assemblies are complicated systems suffering from e.g. fuel crossover across the membrane, non-electrochemical contributions to the cell-voltage and an unknown and variable catalyst utilization factor.[30] Since these measurements leave the performance of individual NPs poorly understood, they are often complemented with studies on model catalysts. Model catalysts have tended to consist either of well-defined macroscopic metal electrodes, or well-characterized dispersions of metal NPs on catalytically inert electrodes. However, there are several recent developments that have allowed the focus of the research to shift towards the study of individual NPs (Fig 2.1c), and such approaches may ultimately provide the missing link between macroscopic electrodes and NP assemblies via single NP activity measurements, as we highlight in this chapter.

The use of NPs or nanoscale electrodes (NSEs) in electrochemistry has been the subject of various recent reviews, focusing on electroanalysis,[15] NSEs and nanopores, [31–33] or NP synthesis.[34, 35] In this chapter, we focus primarily on electrocatalysis at the level of individual NPs, assessing recently developed methodology, including: advances in NP synthesis that allows the rational design of shape-controlled (faceted) NPs; novel electrochemical scanning probe methodologies that allow the study of single NPs; and recent developments in single NP detection. To put these and other studies into perspective we discuss and advocate procedures for reproducible and meaningful experiments. Thus, we identify best practice in both highly defined nanoparticulate electrocatalysis and single NP electrochemistry.

The structure of this review is as follows. First, we briefly outline a number of important and commonly studied reactions in electrocatalysis that are referred to throughout the review, highlighting the present status and outstanding issues. We then discuss common NP synthesis methods and protocols for setting up reproducible measurements of electrocatalysis. This is followed by an assessment of recent results from electrocatalytic measurements on ensembles of NPs where there is a high degree of control over particle shape or mass-transport conditions. These model studies in many ways represent the recently established start-of-the-art. Finally, we give detailed

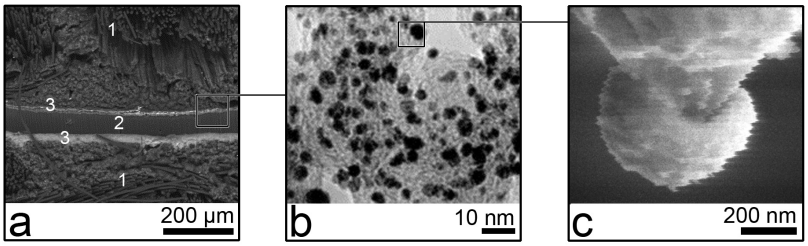

Figure 2.1: Different measurements on electrocatalysts: (a) a real catalyst in application environment,[36] as revealed by a cross section of a complete membrane-electrode assembly (fibrous carbon cloth gas-diffusion layers (1) sandwich a membrane (2) that has both anode and cathode catalyst layers (3) deposited on its sides, appearing as bright gray) (©2004, Elsevier); (b) a commercial Pt on C catalyst as used in studies of model environments.[37] (©2005, Elsevier) (c) an individual, model Pt NP in a model environment. [38] (©2003, American Chemical Society)

attention to emerging frontier techniques that are able to target single NPs, and in the best cases relate structure and activity at a single NP. The chapter concludes by summarizing the main issues and by providing an outlook for the further development of this important field.

2.1.1 Important reactions

Fuel cell reactions are among the most studied electrocatalytic reactions, and we will frequently make reference to them. It is thus useful to give some background on selected reactions, to indicate critical issues involved in respect of electrocatalysis, and the relationship of activity to NP properties.

Oxygen reduction reaction (ORR)

The electroreduction of oxygen is critical to the efficiency of (hydrogen) fuel cells[39] and metal-air batteries.[40, 41] The thermodynamic equilibrium potential for the ORR is 1.23 V versus the reversible hydrogen electrode (RHE), but even on the most active catalyst materials (Pt group metals) significant current is only measured at potentials less than 0.9 V.[42] Recent theoretical studies have provided new insights into the origins of the slow ORR kinetics;[28, 43] the binding energy of the several oxygen-containing intermediates with the electrode surface is key, and platinum surfaces appear to provide interaction energies close to the theoretical optimum.

The full reduction of oxygen to water entails the transfer of four electrons in steps that are depicted schematically in Figure 2.2. The present view is that the predomin-

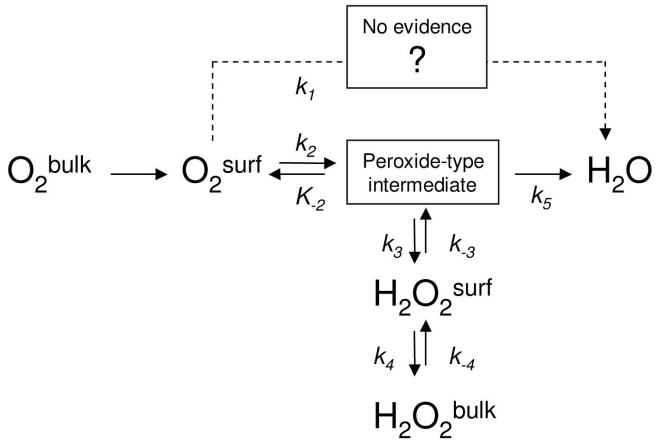

Figure 2.2: A proposed mechanism for the oxygen reduction reaction (ORR).

ant mechanism involves an adsorbed hydrogen peroxide-type intermediate that may convert to and desorb as H_2O_2, before undergoing further reduction. This reduces the effective cathodic current, contaminates the surroundings of the catalyst, and corrodes the polymer membrane present in fuel cells; the formation of hydrogen peroxide is therefore triply undesired. Because on Pt surfaces the oxygen-oxygen bond can be broken, with relatively little interference of the formation of an irreversible oxide, Pt is the best monometallic electrode material for the ORR. In contrast, on very noble metals such as Au, the ORR does not proceed appreciably beyond the reduction to hydrogen peroxide. Transition metals, on the other hand, are prone to form stable oxides, leaving the dissociated oxygen immobilized.[43]

The structure sensitivity of the ORR on Pt has been investigated through the use of single-crystal electrodes. In sulfuric and phosphoric acid solutions, the structural sensitivity of the ORR mirrors the relative adsorption strength of the electrolyte anions, which adsorb strongest on the (111) surface that concomitantly shows the lowest ORR activity.[44] In perchloric acid solutions, anion adsorption does not occur, and the ORR activity is significantly increased.[44] A detailed study of single crystals with varying terrace length has shown that ORR activity increases with increasing step density (i.e. decreasing terrace width), with infinite (111) terraces having the lowest activity,[45] but the absolute difference in activity between different crystal structures is much less pronounced than in sulfuric acid. Although studies of this type provide valuable fundamental information, the projection of these findings to predict NP shape and size

effects in the ORR is not straightforward.

In terms of NP studies, a prevalent view has been that the ORR activity decreases with decreasing NP size,[5, 30] which has been rationalized by the suggestion that the main contribution to the ORR comes from the fraction of extended terraces on NPs, which is increased at larger NPs.[46] However, this view opposes the experimental findings on single crystals outlined above,[45] highlighting the difficulty of translating information between NP studies and macroscale measurements for the ORR. Watanabe et al. have argued that apparent NP size effects on ORR activity can be impacted by experimental design, and, particularly, diminished mass-transport to individual NPs in an ensemble as the particle loading increases.[47] With high NP loadings on a support, recent findings indicate that hydrogen peroxide generated at the NP may re-adsorb on neighboring NPs in close proximity and thereby improve the overall ORR yield.[48]

The influence of both NP size and diffusion effects on the ORR are an important topic of debate, and we will discuss herein recent efforts to study this reaction at individual NPs (Section 2.5), as well as at NP ensembles under conditions of well-controlled mass transport (Section 2.3).

Hydrogen evolution reaction / hydrogen oxidation reaction

The hydrogen oxidation reaction (HOR) is the fuel consuming reaction in fuel cells and the hydrogen evolution reaction (HER) is the cathodic reaction in electrolyzers used to produce hydrogen. Both reactions are characterized by extremely fast kinetics on platinum electrodes[49] and almost perfect reversibility (particularly compared to the complete lack of reversibility of the oxygen reduction and evolution reaction). While the best catalyst for both reactions, Pt, has been known for centuries, materials research to improve HER/HOR focuses on reducing or removing altogether the Pt content, or on modifying Pt to increase resilience towards carbon monoxide,[50–52] a common feedstock contaminant in H_2 produced by steam reforming of hydrocarbons, that is used for fuel cells. The following steps describe the HOR:[30]

$$H_2 + 2\,{}^* \longrightarrow H_{ad} + H_{ad} (\textit{Tafel reaction}) \tag{2.1}$$

$$H_{ad} \longrightarrow {}^* + H^+ + e^- (\textit{Volmer reaction}) \tag{2.2}$$

$$H_2 + {}^* \longrightarrow H^+ + H_{ad} + e^- (\textit{Heyrovsky reaction}) \tag{2.3}$$

where * indicates a vacant site at the catalyst surface. Definitive determinations of the mechanism and NP size dependence have remained elusive due to the complica-

tions posed by the fast kinetics of the HOR.

The counterpart HER reaction is not hindered by mass-transport in the high-proton concentrations of acidic electrolytes relevant for electrolyzers. On the macroscale, the Pt (110) surface is the most active,[44] while HER activity has been observed to increase with decreasing particle size,[53, 54] as discussed in more detail in Section 2.5.1. On Pt, it is well established that the HER follows a Volmer-Tafel mechanism.[30]

Hydrazine oxidation

Hydrazine (N_2H_4) is a potent fuel that can be oxidized to form molecular nitrogen and water in a four-electron reaction. The reaction proceeds very rapidly via successive deprotonation steps that leave the N-N bond intact.[55, 56] On Au there is an overpotential of almost 500 mV with respect to Pt,[56] but for both metals, once the onset potential is reached, a mass-transport limited situation is readily established with further increasing potential. Carbon electrode materials are essentially completely inactive towards hydrazine oxidation. Due to this strong dependence of the onset potential on the type of electrode material, as well as the fast reaction kinetics, hydrazine oxidation has proven very suitable to distinguish between different electrode materials, making it a good redox probe for NP collision experiments that are discussed in Section 2.5.2.

2.2 Preparation and characterization of nanoparticulate electrocatalysts

A key aspect to the study and employment of NPs as electrocatalysts is the preparation and characterization of nanoparticulate electrodes, which often consists of NPs dispersed on a (typically non-electrocatalytic) support material. In such electrodes, the NP support plays a number of roles. First and foremost, from a practical point of the view, the support electrode acts as a conductive bridge, contacting the NPs to an external electronic circuit. Second, the support acts to disperse the NPs, to limit agglomeration and maintain the high surface-to-volume ratio desired. Finally, the interaction between the support material and the NPs can be employed to modify the electrocatalytic activity of the NPs.[57] For example, Hayden et al. showed that titania-supported Au NPs have higher activity for the electrochemical oxidation of CO than carbon-supported Au NPs,[57] while titania-supported Pt NPs are less active for CO oxidation[58] and oxygen reduction[59] than carbon-supported Pt NPs. Although the occurrence of such support effects is well-known in gas-phase heterogeneous

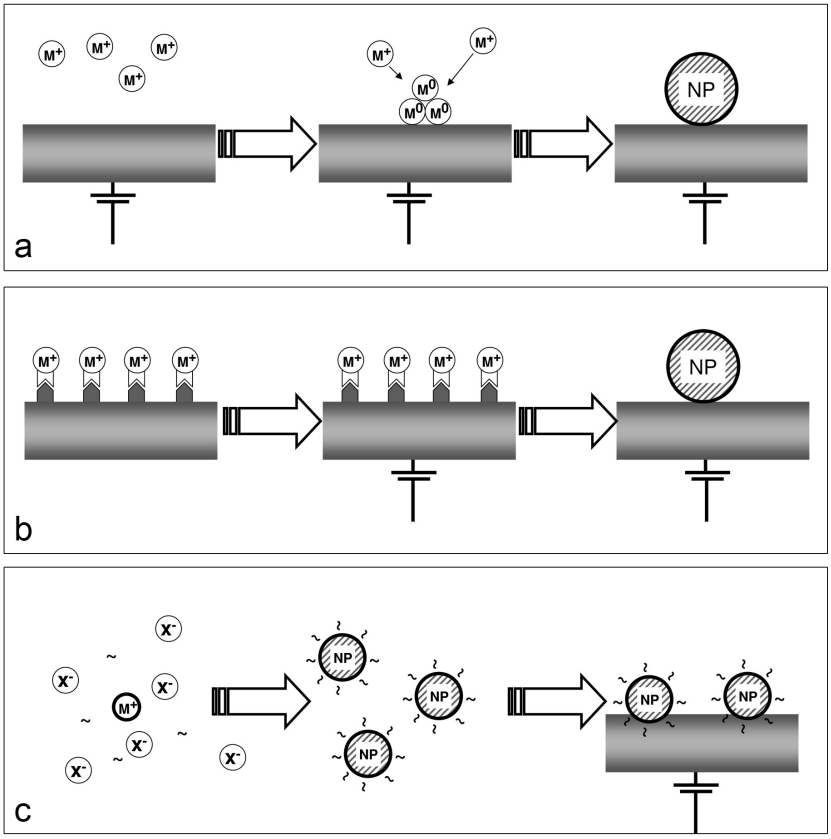

Figure 2.3: Three general approaches to fabricate a nanoparticulate electrode: (a) simultaneous NP formation and immobilization; (b) immobilization of metal ions followed by reduction; (c) synthesis of metal NPs followed by their immobilization.

catalysis,[60–63] the interplay between the support material and NP activity is significantly less understood in electrocatalysis.

The most common support materials are various types of carbon[64–68] as the electrodes used in fuel cells are typically carbon-based. In addition, carbon is cheap and relatively inert towards many electrocatytic (bond-breaking and bond-making) processes. For fundamental studies, gold has found considerable use as it can be cleaned and characterized easily, and provides a stable surface.[69, 70] Titania has also received attention as a model in studies of support effects,[57, 59] while doped tin oxides are typically employed as support materials for applications where optically transparent electrodes are desirable.[71–73]

While there are numerous methods to prepare and immobilize NPs on conductive

supports, they broadly fall into three categories (Figure 2.3): a) simultaneous (single-step) NP formation and immobilization; b) immobilization of metal ions followed by their reduction to metal NPs; c) synthesis of metal NPs followed by their immobilization on the surface of the support electrode.

2.2.1 Single-step nanoparticle formation and immobilization

In this approach, the formation and immobilization of NPs on a support electrode takes place simultaneously in a single-step. Examples of this approach are: the electrodeposition of NPs from a solution containing the metal ion, either onto the bare support electrode,[74–82] or onto the support electrode modified with a polymer film;[78, 83–86] electroless deposition;[77, 87, 88] and vacuum evaporation.[89–93] Electrodeposition is by far the most popular of these methods, as it makes use of electrochemical equipment, ensures an electrical contact between the NP and substrate and provides many tunable parameters, such as the deposition potential or current, time, temperature and electrolyte composition,[74, 75, 94] to adjust the size-, shape- and spatial distribution of the electrodeposited NPs. The coupling of electrodeposition experiments with other characterization techniques, such as ex situ[95–97] and in situ TEM,[98, 99] and small-angle X-ray scattering (SAXS)[100] has provided valuable insights into the early stage of NP formation which may ultimately lead to improved electrodeposition protocols.

The main drawback of electrodeposition at present is that it typically leads to NP deposits with a wide size distribution,[74] for three reasons. First, new NP nuclei (small clusters of atoms) may form during the entire duration of the electrodeposition process (progressive nucleation).[74, 76] This leads to a wide distribution in growth times for individual NPs, and, consequently, in NP sizes. Second, during growth, depletion layers of neighboring NPs can start to overlap, causing these NPs to grow more slowly compared to those which are diffusionally isolated.[101] Consequently, the size of a single NP correlates with the local number density of NPs. As the number of nearby NPs will vary from one NP to the next in a random ensemble, this leads to a broadening of the size distribution during NP growth.[101] Third, (surface mediated) Ostwald ripening can occur, whereby large NPs grow at the expense the small NPs due the size-dependence of the free energy of stabilization of a NP.[102, 103]

To circumvent the size dispersion due to the progressive formation of new nuclei, efforts have been made to separate in time the formation of nuclei, and the growth of those nuclei. This control is typically achieved by forming nuclei with a short (< 10 ms) potential pulse at high overpotential with respect to the reduction potential

of the metal ions in solution, followed by a long growth pulse (up to minutes) at low overpotential, where no new nuclei are formed and all growth occurs on pre-formed nuclei.[71, 74, 75, 77, 104–109] Slow NP growth at low overpotential also diminishes concentration polarization near the substrate, so that local NP coverage has less effect on the extent of growth of individual NPs. This double potential pulse approach has been successfully employed to electrodeposit reasonably monodisperse NP arrays of various metals.[71, 74, 75, 77, 104–109]

An alternative method to minimize depletion effects is to incorporate a local source of convection within the depletion layer. An easy way to achieve this is to drive a gas-evolving reaction (in practice through the co-evolution of hydrogen from protons), in parallel with the electrodeposition reaction, so that the formation and release of gas bubbles drives convective mixing near the growing NP.[110, 111] While H_2 co-evolution leads to the size distribution narrowing,[110] the resulting NPs are typically nanocrystalline and fractal in nature.[110, 111] Finally, the deposition of NPs in a periodic array, ensures that mass transport to each NP is similar.[112] However, this method is rarely employed, as it involves extensive pretreatment of the substrate electrode to create a periodic array of nucleation sites.

2.2.2 Immobilization of metal ions followed by reduction

In this two-step procedure, metal ions are immobilized on the electrode surface before being reduced (either chemically or electrochemically) to form NPs directly attached to the surface. The spatial distribution and average size of the resulting NPs are determined by the amount of metal precursor, which can be controlled by adjusting the density of metal ion immobilization sites. By limiting the amount of immobilized ions, the preparation of small NPs is facilitated.

A key challenge of this approach is the controlled introduction of functional groups that coordinate to the desired metal precursor on the electrode surface. One option is to immobilize ions within a polyelectrolyte film deposited onto the substrate electrode,[113–118] leading to the encapsulation of NPs within the polyelectrolyte film. While this encapsulation provides a steric barrier to particle agglomeration, the resulting NPs may be less catalytically active than bare NPs.[113] An alternative method to functionalize the support electrode is diazonium coupling,[119–123] which can be performed on many electrode surfaces (metal, semiconductor, carbon), but is most commonly employed on carbon electrodes (such as highly oriented pyrolytic graphite (HOPG),[107] and carbon nanotubes[124–126]).

2.2.3 Synthesis of metal nanoparticles followed by immobilization

Optimal control of NP size and shape can be achieved by separating NP formation from the immobilization step, by synthesizing NPs in solution and then attaching the NPs to the support electrode. NPs in solution are most often prepared by colloidal synthesis, an empirical method which offers excellent shape and size control, and requires simple equipment. A rich body of literature has developed since the seminal work by Turkevich,[127] followed up by Brust, Bethell, Schiffrin and co-workers.[128] The principle of colloidal synthesis is straightforward and, in general terms, three components are required for the synthesis: a metal precursor (metal salt) which provides the metal ions, a reducing agent (such as H_2, BH_4^- or citrate) which reduces the metal ions to metal atoms to form NPs, and a stabilizing agent (such as citrate or various polymers) which limits the size and prevents the NPs from agglomerating. Solutions of the three chemicals are mixed together, causing formation of metal nuclei, which grow by the addition of atoms.[129] The equilibrium shape of a NP, as predicted by the Wulff theorem, is a polyhedron and, at a larger radius, a sphere.[130] The final morphology of the particle can be altered by controlling the kinetics of the growth, for example, by adding surfactants that bind preferentially to specific surface facets, thereby slowing their growth rate.[131, 132] Controlling the conditions allows the tailored synthesis of shape-selected NPs, with specific surface facets exposed, which is beneficial to the catalysis of selected reactions, as described further in Section 2.4.[35, 131–133]

The colloidal synthesis of dendrimer encapsulated NPs is an interesting approach that brings additional control options.[67, 134–140] Dendrimers are hyperbranched, highly regular macromolecules, consisting of a central core from which branched (monomer) units extend.[141, 142] In this approach, metal ions are trapped at functional groups within the well-defined dendrimers before being reduced to the corresponding metal NP. Conceptually, this is similar to the ion-immobilization/reduction approach described above, with the main difference being that the dendrimer is in solution-phase rather than tethered on the electrode surface. Dendrimers are attractive for NP synthesis for a number of reasons. (1) The dendrimer templates can be synthesized with a high degree of control by defining the number of generations (number of 'layers' of monomer units) in the dendrimer synthesis, and the number of ion-anchoring functional groups can thus be controlled. This allows NPs to be synthesized from less than 1 nm to up to 4-5 nm by the number ion-anchoring groups, with a relatively narrow size distribution.[67, 134–140] (2) The NPs are encapsulated within the dendrimers, which serve as stabilizing agents to prevent agglomeration. (3) The open dendrimer struc-

ture and the fact that NP stabilization is mainly due to steric effects leaves a significant fraction of the NP surface available for catalytic reactions. (4) The dendrimer branches can be functionalized to act as selective gates to the NPs. (5) The terminal groups on the exterior of the dendrimer branches can be modified to control the solubility of the dendrimer encapsulated NP or to tether it to electrode surfaces.[143]

An alternative, novel method of NP fabrication has been recently reported under the name 'cathodic corrosion'. In this electrochemical method, Yanson et al. demonstrated that NPs of various metals (including Pt, Au, Cu, Ag, Ni, Rh, Si, Nb, and Ru) and metal alloys (PtRu, PtIr, PtNi, AuCo, AuCu, and FeCo) can be formed from pristine metal wires by simply applying very negative potential of ca. -5 or -10 V to the metal in an aqueous electrolyte containing a strong non-reducible cation, hence the name 'cathodic corrosion'.[144, 145] Application of an alternating voltage aids in dispersing the NPs but is not essential to their formation. Furthermore, it was shown that by tuning the electrolyte concentration and the electrical current, the shape and size of NPs could be controlled.[146, 147] A major advantage of this method is that it offers a similar degree of shape and size control as the colloidal synthesis of NPs, but does not require a stabilizing agent or other additives during the synthesis, leaving the NPs clean. Furthermore, this method is versatile, as it allows the fabrication of NPs of almost any metal and metal alloy.

In order to employ synthesized NPs for electrochemical studies, one needs to immobilize them on the surface. Furthermore, some stabilizing agents on the NP surface may need to be removed to avoid interference with the NP reactivity. The most common method to attach solution-dispersed NPs to support electrodes is by simple drop-casting: an aliquot of a NP-containing solution is placed on the support electrode, and the solvent is left to evaporate, leaving the NPs behind. While straightforward, drop-casting often leads to inhomogeneous deposition with severe particle aggregation, particularly around the edges of the drops, similar to the 'coffee-ring effect'.[148–150] Furthermore, the NPs are only weakly adhered to the surface through van der Waals forces, and NP detachment can be a significant problem.

An alternative way to tether NPs is to functionalize the support to provide specific anchoring sites for the NPs. This can be done by introducing a layer of functional groups onto the surface of the support electrode, through diazonium grafting (see previous Section), or by functionalization with a self-assembled monolayer (SAM), which is terminated with a functional group that binds strongly to the NPs.[151–168] The formation of SAMs on surfaces is a broad research field that has been reviewed extensively.[169–173] SAMs are spontaneously formed monomolecular layers consist-

ing of a head group that interacts with the surface, a molecular chain of variable length, and a terminating functional group. In the context of this review, three main classes of SAMs should be considered, namely alkanethiols[162–168] and alkyl isocyanides[161] for (coinage) metal surfaces (such as gold electrodes), and alkoxysilanes for metal oxide surface (such as silica or doped tin oxide electrodes).[151–160]

To link to the NPs, the SAMs need to be terminated with a functional group that provides an anchoring site for the NPs. Typically, this functional group is a thiol[151, 158, 160, 162–164, 174], amino[151–156, 158, 167, 168] or isocyanide[151, 161] group, as these have a high affinity for metal NPs through the formation of covalent metal-sulfur or metal-nitrogen bonds, thereby displacing the stabilizing agent present on the NPs. An alternative method of tethering NPs is to imbue a charge, typically by depositing a charged polymer (polyelectrolyte) on the support surface with a charge opposite to that of the NPs, thereby binding the NPs electrostatically.[157, 165, 166, 175] By tethering the NPs to the surface through a linker molecule, a more uniform surface distribution with minimal agglomeration can be obtained,[157, 175] as the binding sites to the NPs are regularly arranged in a quasi-two-dimensional plane.

When using the tethered NPs as electrocatalysts, it is imperative that electron transfer (ET) can occur across the SAM between the NP and the underlying substrate. Classically, in the absence of NPs, ET across an insulating layer is determined by the probability of electron tunnelling through the layer. This probability is proportional to $exp(-\beta d)$, where β is the tunneling decay constant (β ~1 $Å^{-1}$ for saturated hydrocarbon bridges)[165–167, 176–179] and d is the thickness of the insulating layer. Practically, this exponential decay means that hydrocarbon SAMs (such as alkanethiols) with chains longer than about 10 carbons would essentially completely block ET between species in solution and the electrode surface, and no Faradaic electrochemistry from the redox species in solution would be observed, as has been amply demonstrated.[157, 158, 165–167, 174, 180, 181] Interestingly, the adsorption of NPs on top of the SAM opens up a pathway for ET across the SAM, which was found to be as efficient as in absence of a SAM.[157, 158, 165–167, 174, 180, 181] The groups of Fermín[165, 166, 182] and Gooding,[167, 174, 180] have shown in a series of systematic studies that NP-mediated ET appears to be relatively distance-independent (i.e. β ~0) for typical SAM layers and, furthermore, that ET between the redox species and the NP is the rate-limiting step (rather than ET across the layer).

These findings have been rationalized in a theoretical description of NP-mediated ET by Chazalviel and Allongue.[183] This theory considers ET between: (1) a redox couple and a metal electrode (represented by the exchange current density J_0); and

(2) a metal NP and a metal electrode (represented by the exchange current density J_1) (Figure 2.4a). Typically, J_1 is about twelve orders of magnitude larger than J_0, unless a NP is particularly small.[183] The introduction of an insulating layer, such as a SAM on the electrode, causes a decrease in the ET rate proportional to exp(-βd) (see above). Typically, J_1 is sufficiently large that even J_1 exp(-βd) is still much larger than J_0, and adsorption of NPs thus opens up an effective ET pathway across the SAM. An important consequence of this model is that NP-mediated ET is unimpeded by the presence of a SAM as long as the NP is relatively large compared to the thickness of the layer (Figure 2.4b), a prediction which has been validated experimentally by Gooding et al. (Figure 2.4c).[180]

Importantly, the Chazalviel-Allongue theory[183] demonstrates that for NPs tethered to an electrode surface through a SAM, ET across the SAM is only impeded in the case where the NPs are very small (and very monodisperse, as a few NPs above the critical size could already provide an efficient ET pathway), or the SAM is rather thick. Otherwise, NP tethering is an efficient way to immobilize NPs on a support electrode with minimal NP aggregation or desorption, which can also be applied to study electrocatalytic processes.[157]

2.2.4 Cleaning

When a nanoparticulate catalyst is prepared using surfactant-free techniques such as vacuum deposition, electrodeposition, electroless deposition or cathodic corrosion, additional cleaning steps are often not required. Colloidal NPs, however, necessarily have a layer of surfactant molecules on their surface. Since this surfactant film could inhibit the adsorption of reactants in catalytic reactions,[184] it needs to be removed as part of the catalyst preparation.

Solla-Gullón et al. demonstrated the use of CO adsorption at surfactant-coated Pt NPs as a method for NP cleaning.[185] Since CO adsorbs preferentially on Pt, the surfactant is displaced by a monolayer of CO, which can then be stripped off the surface electrocatalytically in a subsequent oxidative potential sweep. The cleanliness of the surface can then be assessed through electrochemical characterization of the nanoparticles, as discussed below. While CO gas should be handled with caution, this method is very successful at cleaning NP surfaces and can be applied to all metals that adsorb CO strongly; for example for the cleaning of Pt[185] and Pd NPs.[186]

An alternative cleaning method was reported by Rodriguez and Koper,[187] showing that the surface of Pt NPs capped with polyvinylpyrrolidone (PVP) can also be cleaned with a diluted sulfuric acid solution containing H_2O_2, leaving a clean Pt sur-

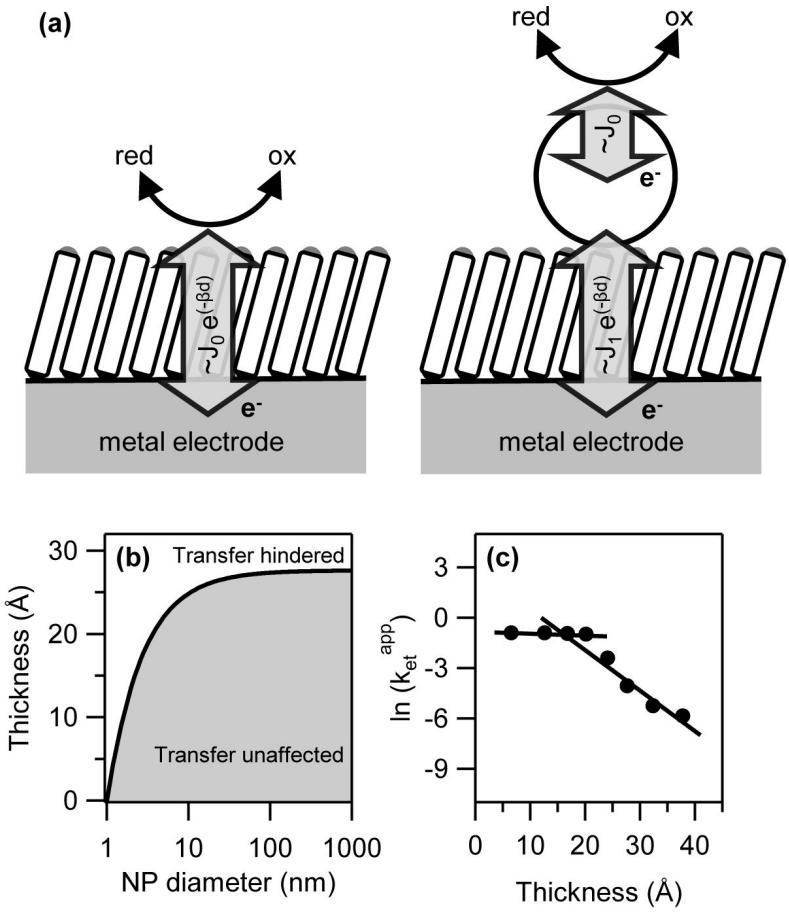

Figure 2.4: a) Schematic comparison of electron transfer between a redox couple and a support electrode across a SAM (left) and nanoparticle-mediated electron transfer (right) Adapted from reference [183]. ©2011, American Chemical Society. (b) Theoretical prediction of the critical thickness of an insulating layer (between a collector electrode and a metal NP) which leads to a change in the voltammogram of a reversible system in solution as compared to a bare metal electrode(adapted from ref [183].) (c) Variation in the apparent electron transfer kinetic constant for the one-electron reduction of $Ru(NH_3)_6^{3+}$ to $Ru(NH_3)_6^{2+}$ on 27 nm AuNPs with the thickness of an insulating poly(ethylenediame) layer. Adapted from reference [180]. ©2012, American Chemical Society

face (as characterized electrochemically). Importantly, it was found that this method leaves the superficial order of the NPs intact. It was suggested that the decomposition of hydrogen peroxide on the Pt surface creates oxygen gas bubbles at the NP surface that physically displace the PVP molecules.

The Alicante group of Feliu have also studied the effect on NP surface structure of cleaning catalyst layers using a UV/ozone treatment,[188] as this was reported by Somorjai et al. to increase the catalytic activity of colloidal particles in gas phase catalysis.[189] Through voltammetric analysis, it was found that ozone treatment actually severely perturbs the original surface structure of the NPs, in a way similar to the changes in surface structure resulting from electrochemical oxygen adsorption.

2.2.5 Characterization

After surface adsorbates have been removed from NPs, it is important to determine the NP shape and size and the total NP surface area exposed to the electrolyte. These characteristics can be determined by a combination of techniques that can be roughly divided into electrochemical and non-electrochemical methods.

Electrochemical Characterization

A very accurate way to determine both the exposed surface area and the dominant surface structure of noble metal electrodes is through the study of adsorbed monolayers of atomic or molecular fragments. Examples are the underpotential adsorption and desorption of hydrogen on Pt surfaces (H_{UPD}) and the formation of oxide monolayers.[190, 191] The amount of surface atoms exposed to the electrolyte, or the electrochemically active surface area,[192] can be determined from the charge passed during the adsorption or desorption of a monolayer. Moreover, the voltammetric signature for monolayer formation or monolayer 'stripping' can be very sensitive to the surface structure, as has been shown for hydrogen adsorption/desorption on Pt single crystal electrodes.[190] When applied to nanoparticulate electrodes, an average NP shape can be deduced, from the relative amounts of surface facets measured using such techniques (Figure 2.5).

The analysis of Pt NP shape and surface structure through electrochemical characterization has been extensively developed by the Alicante group.[70, 193] To identify the ratio of the various exposed surface facets on shape-selected Pt NPs, site-specific irreversible adsorption of adatoms was employed. Specifically, it was shown that bismuth and tellurium adsorb selectively on (111) terraces of more than 3 atoms width,

while germanium adsorbs selectively on (100) terrace sites. After adsorption, these adatoms can be stripped, revealing quantitatively the amount of adsorption, and hence values for the amount of each surface. By this method, the relative fractions of (111) and (100) sites were determined for NPs of various shapes, and found to be in agreement with the analysis of the shape of NPs obtained by TEM measurements.[70] Recently, the group reported a detailed characterization of the surface domains on Pt NPs by careful measurement of the hydrogen adsorption and desorption region, as well as the oxidation of CO, in sulfuric acid, perchloric acid and sodium hydroxide electrolytes.[193]

There are fewer reports on the electrochemical characterization of NPs of metals other than Pt, although some methods are noteworthy. The voltammetry of Pd in sulfuric acid also exhibits electrochemical signals corresponding to the adsorption and desorption of monolayers of oxide and hydrogen, that can be used for structure-sensitive determination, and this has been used to characterize Pd NPs.[186] The Alicante group reported the electrochemical determination of the surface structure of Au NPs via the underpotential deposition (UPD) of Pb.[194] The voltammetric signal of Pb UPD is surface sensitive and shows contributions from the three Au basal planes. Nanoparticulate Ru electrodes can be characterized using CO stripping and Cu UPD.[195] In general, CO stripping can be used to determine the electrochemically active surface area of a range of metal NPs.[196–199]

Non-electrochemical characterization

The size and/or shape of NPs may be evaluated through several techniques. Atomic force microscopy (AFM) and X-ray diffraction (XRD) are relatively easily used to estimate NP size. AFM is a scanning probe technique that is highly sensitive to height changes out of the plane.[200] However, its lateral sensitivity is not sufficient to detect the shape of (small) NPs, but the height change with respect to the plane can be taken as the diameter of a NP.[200]

The width of diffraction peaks in XRD is related to the size of the average crystallite in the sample under study, and in the case of (small) NPs it can be assumed that each NP consists of a single crystallite and the NP diameter can then be found via the well-known Scherrer equation.[201] It should be noted that the Scherrer equation depends on the crystallite shape (e.g. spherical or cubic), so that high precision size measurements can only be made by XRD when another microscopic technique is used to determine the NP shape.[201] Since the Scherrer equation yields the average crystallite size, XRD is not a good means to estimate the dispersion of NP sizes.

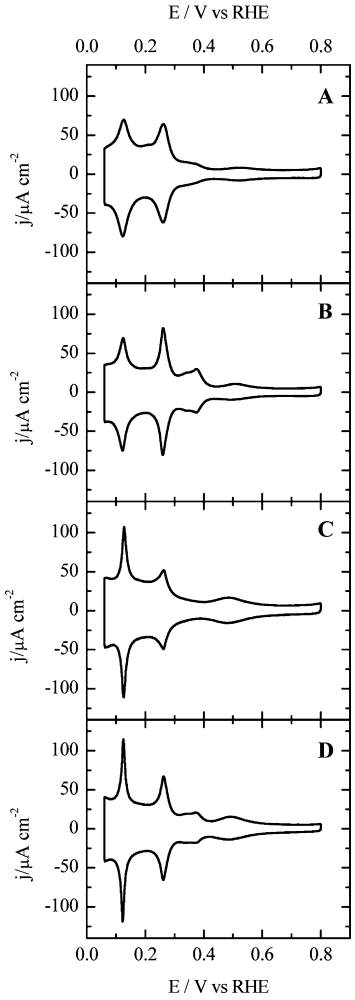

Figure 2.5: Cyclic voltammograms corresponding to (a) spherical (polyoriented), (b) cubic (rich in (100)-type sites), (c) octahedral and tetrahedral (rich in (111)-type sites), and (d) truncated octahedral and tetrahedral (rich in (111)-type and (100)-type sites) Pt NPs in 0.5 M H_2SO_4 (50 mV s^{-1}). Voltammetric features related to different types of sites: peak at 0.125 V for (110)-type sites, peak at 0.27 V containing contributions from (100) step sites on (111) terraces and sites close to steps on the (100) terrace, broad peak at 0.35 – 0.37 V for (100) terraces, and a broad peak at 0.5 V related to (111) terraces. Adapted from reference [193]. ©2012, American Chemical Society

Furthermore, a number of optical methods can be used for NPs with a large photon scattering cross-section for rapid size determination, such as dynamic light scattering (DLS)[202] and NP-tracking analysis (NTA).[203] In DLS, a laser beam is shone through a dilute solution of colloidal NPs, and the light transmission is measured as a function of time. The NPs in solution act as point scatterers. As the NPs move in solution due to Brownian motion, the interparticle distance changes, giving rise to either constructive or destructive interference of the scattered light by surrounding NPs, which causes fluctuations in the transmission. The timescale of these fluctuations can then be correlated with the timescale of the movement of the NPs, from which the diffusion coefficient, and, through equation 2.6 (Section 2.5.2), NP size can be extracted. It should be kept in mind that this analysis is complex, especially for a polydisperse sample. Like DLS, NTA exploits the fact that NPs in solution acts as point scatterers.[203] However, rather than inferring the motion of NPs from the overall intensity of the transmitted light through a NP solution, NTA follows the Brownian motion of NPs directly in real-time. This is done by mounting the cell containing a solution of NPs onto an optical microscope, equipped with a high speed CCD camera, which allows the visualization of the position of individual scatterers (NPs) when a laser beam is passed through the sample. By following the position of many NPs separately over time (typically less than a minute), the average distance moved by individual NPs is calculated, and the size of each individual NP is derived to construct a size distribution.

Importantly, both DLS and NTA rely on measuring the intensity of scattered light, which for NPs much smaller than the wavelength of the incident light can be described by Raleigh scattering.[204] The scattering cross-section is dependent on the refractive index of the material and very strongly dependent on NP size, which limits the applicability of light-scattering based techniques to the characterization of relatively large NPs (> 10 nm) of highly refractive materials, such as gold, silver, and, to a lesser extent, other metals.[204]

Finally, UV-visible absorption spectroscopy can be employed for the size determination of NPs of metals for which the wavelength of absorbed light depends strongly on the particle size. In practice this method is mostly limited to Au and Ag NPs.[205, 206]

To judge the particle size with certainty and visualize the average particle shapes obtained in the synthesis, transmission electron microscopy (TEM) measurements are required. No other measurement technique gives the accuracy level of TEM, which, in modern, high-resolution versions, even allows for the determination of the exposed crystal surface facets per particle.[207] Interestingly, the use of high-resolution TEM combined with electron tomography can accurately image single NPs as well as NP

clusters and has helped in elucidating the growth mechanism of electrodeposited NPs.[96]

2.3 Model approaches to real catalysts

As has been pointed out in the Introduction, it is extremely difficult to extract even the intrinsic (average) activity of NPs from measurements on real catalysts (Figure 2.1a). In this section we discuss approaches that have been developed to mimic the mass transport conditions of fuel cell electrodes and studied the influence of mass transport on catalyst performance in model systems. In the best situations, such experiments use NPs of very well defined size, and/or inter-particle distance. Moreover, the use of flow cells offers a high degree of control over the mass transport of reactants to arrays of NPs. This type of measurements thus allows the accurate evaluation of important catalyst parameters such as the effect of particle size or of catalyst loading on rates and reaction pathways.

2.3.1 Influence of mass-transport

The nature of mass transport towards a nanoparticulate electrode is schematically indicated in Figure 2.6. When the support material is inert, a radial concentration gradient forms from the NPs performing the electrocatalytic reaction creating 'diffusion spheres'. The distance from the electrode where the concentration is 90% of the bulk concentration (or, technically, 90% of the bulk concentration minus the surface concentration) can be considered as the thickness of the diffusion sphere. Overlap between the diffusion spheres leads to the formation of a continuous diffusion layer, and the electrode effectively acts as a planar electrode (Figure 2.6a).

Catalyst NPs in real devices experience rather complex mass transport regimes, critically depending on the interparticle distance, which in turn depends on both the NP size and loading. As the inter-NP distance decreases, there is increasing diffusional overlap between adjacent particles in terms of both reactant diffusion and intermediate/product transport (Figure 2.6b). One particular impact on catalysis that has been seen in the ORR is that the diffusion-limited flux of oxygen to individual NPs in an array decreases and thus the apparent catalytic activity of each NP.[47] The loading of NPs, and the impact on mass transport, is thus an important factor that needs to be accounted for when trying to compare intrinsic NP activities in different studies.

Behm and Kasemo and co-workers have suggested that, for the ORR, overlapping diffusion spheres may also enhance overall catalytic activity.[48] The mechanism of

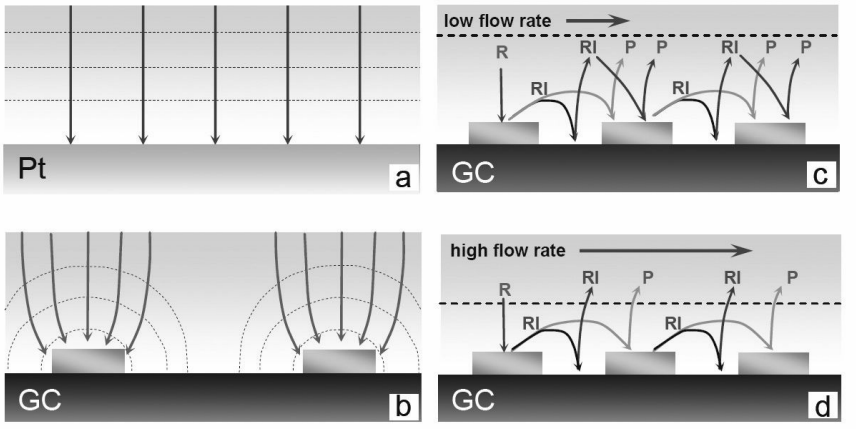

Figure 2.6: Mass transport towards electrodes: diffusion towards an infinite planar electrode is linear (a), while well-separated NPs show radial diffusion spheres (b). As the inter-NP distance is decreased, the diffusion spheres start to overlap. In (c) and (d), the influence of flow rate on mass transport to a NP array is illustrated: at low flow-rate, the diffusion layer is large and there is a chance for reaction intermediates (RI) generated at a NP to re-adsorb on adjacent NPs (c). When the flow-rate is increased, the diffusion layer effectively becomes thinner and RIs are less likely to re-adsorb, escaping from the NP ensemble (d). Adapted from ref [208]. ©2010, The Electrochemical Society.

ORR can proceed via hydrogen peroxide as an (adsorbed) intermediate (reaction k_3 in Figure 2.2) and this species may desorb from the catalyst surface instead of reacting to water, leaving the oxygen reduction incomplete. This aspect of the ORR is also considered below for measurements on individual Pt NPs (Section 2.5.1). In an ensemble, if NPs are in close proximity, there is an increased chance that hydrogen peroxide produced on one NP re-adsorbs on an adjacent NP, and is reduced further to water, as illustrated in Figure 2.6 (c) and (d).[48] The chance that a reaction intermediate will readsorb depends on the degree of overlap of the diffusion zones of adjacent NPs. This diffusion sphere overlap can be predicted numerically[209, 210] and also visualized using fluorescence confocal microscopy.[211]

It is apparent from the foregoing that studying the dependence of NP loading and inter-particle distance for highly organized NP arrays is hugely beneficial towards uncovering any subtle influences of NP loading on electrocatalysis. Behm and Kasemo et al. used lithographical techniques to fabricate an array of ~100 nm Pt disks on a carbon electrode, that was deployed as a working electrode in a flow cell system, similar to the one shown in Figure 2.7.[212] The effect of mass transport rate could be investigated by: (i) varying the flow-rate of electrolyte over an ensemble of Pt nanodisks (Figure 2.6 c, d) and (ii) varying the radii and inter-particle distance (Figure 2.6b). Increasing the flow-rate (decreasing the diffusion layer thickness) or the inter-particle distance serves to diminish diffusional coupling between neighboring NPs and thus reduces the chance of re-adsorption of RIs.[213] In this setup, a Pt electrode downstream of the Pt NP array was used to quantify the amount of hydrogen peroxide produced.[48] As the NP density was increased and/or the flow-rate was reduced (i.e. the mass transport rate was reduced), the amount of hydrogen peroxide detected downstream diminished. The same effect was also demonstrated for other reactions that feature soluble intermediates, such as the methanol oxidation reaction.[214]

The flow cell in Figure 2.7 was used by Dumitrescu and Crooks to study the effect of flow rate on ensembles of well-defined dendrimer-encapsulated Pt NPs supported on microband electrodes.[215, 216] A key attribute to this type of cell is that the hydrodynamics are very well defined and transport can be varied and controlled over a wide range.[213] Two working electrodes, each decorated with dendrimer-encapsulated Pt NPs, were placed adjacent to each other and perpendicular to the direction of electrolyte flow. The downstream electrode served as a 'collector' electrode, and was held at a potential to oxidize hydrogen peroxide, while cyclic voltammetry was used to measure the ORR on the upstream 'generator' electrode. It was found that even at elevated flow rates, the hydrogen peroxide yield (i.e. the fraction of H_2O_2 formed relative to the

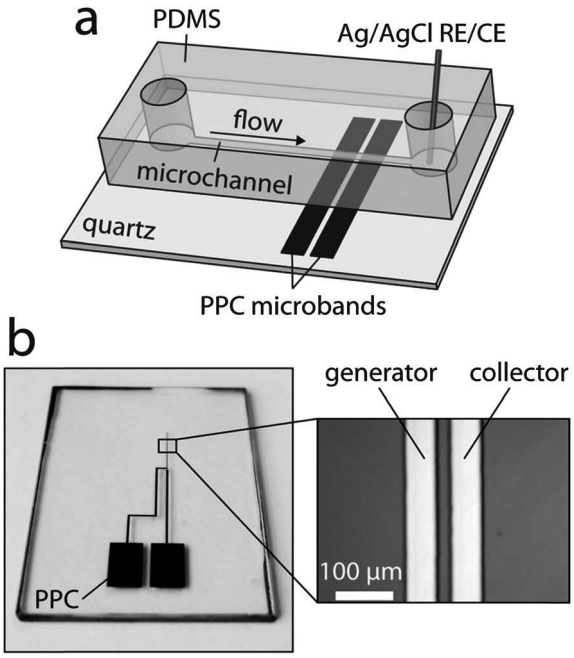

Figure 2.7: Electrolyte in a microchannel in PDMS (polydimethylsiloxane) flows across two pyrolized photoresist carbon (PPC) microband electrodes covered with with dendrimer- encapsulated Pt NPs; the band closest to the flow source is the generator electrode, performing the ORR and any residual products can be collected at the downstream collector electrode. RE: reference electrode; CE: counter electrode. Adapted from [215]. ©2012, Royal Society of Chemistry.

total amount of O_2 consumed) remained constant.[216]

A constant H_2O_2 yield with the flow-rate was also observed by Behm et al. for extended polycrystalline Pt surfaces (see Figure 5c in reference [48]) consistent with the results of Dumitrescu and Crooks.[216] It should be noted that the dendrimer encapsulated NPs were assumed to form a close-packed monolayer, which may be considered as a planar Pt electrode (Figure 2.6a). This indicates that the relative hydrogen peroxide yield during ORR does not increase with increased flow-rate (mass transport) over high-density planar Pt electrodes, but it does increase at increasing inter-particle distance (i.e. lower catalyst loading).

2.3.2 High throughput electrocatalyst screening

Variations in the electrocatalytic activity for different NP sizes or NP loadings within an array, can be screened particularly effectively using a scanning electrochemical microscope (SECM), a powerful technique for mapping the local reactivity.[217, 218] A reactivity map is made while laterally scanning an ultramicroelectrode (UME; electrode with a critical dimension smaller than the diffusion layer thickness) in close proximity to a larger electrode surface under study. Depending on the nature of the electrochemical reaction, the current is measured at the UME or at the substrate electrode. For instance, the change in the ORR reactivity of an array of microdots containing Pd NPs with increasing Co content was mapped by generating oxygen at the scanning UME and measuring the ORR current of the electrode supporting the array.[219]

Many reports have appeared in recent literature, which have applied SECM to assess a range of different material combinations for fuel cell reactions,[220–223] as has been summarized in the recent reviews.[218, 224] While these studies identify appropriate protocols for measuring ORR activity, a careful study of catalyst activity as a function of catalyst loading (inter-NP distance) and NP size by SECM has not yet been performed. In light of the flow cell studies described above, and others, such screening studies could be very interesting, considering the debate concerning the impact of NP size and loading on electrocatalytic activity that is ongoing (see Section 2.3.1). The use of SECM to investigate electrocatalytic activity as a function of NP shape will be discussed in more detail in Section 2.4. It should also be noted that an interesting aspect of SECM is that the substrate does not need to be a biased electrode. One can use the tip UME to generate a reversible electron donor or electron acceptor that couples to an electrocatalytic reaction enabling studies of electrocatalytic NPs on an inert (insulating support). This approach is thus valuable as a means for studying support effects on ET at NPs. The approach has been used to study the HER

at well-defined arrays of NPs in different environments.[225, 226]

A particularly interesting method of model electrocatalyst screening has been reported by the group of Hayden.[227] To deposit a range of different particle sizes in an array, a masked substrate was used in an ultrahigh vacuum physical vapor deposition (PVD) chamber. Using a PVD source, thin films of single metals or metal alloys (by simultaneously using multiple sources) could be deposited, and by imposing a shutter to partially shadow the source, a range of deposition rates was obtained at different locations on the substrate.[228] Interestingly, if the deposited films were sufficiently thin, they formed nanoparticulate islands rather than a planar film. In this way an array of different NP sizes could be easily generated, since the film thickness varied over the length of the substrate.[229] For these investigations, the substrate was an array of 100 planar microelectrodes (0.8 mm^2) of ternary alloys (such as PdPtAu and TeGeSb) that were individually addressable, each with a different, but well-defined composition.

This approach was applied to the ORR at Pt NPs. For NP sizes from 7 nm to 1 nm the specific activity was shown to decrease sharply.[227] However, it should be noted that with the PVD technique used, the distance between NPs decreased as the particle NP size was increased. Following on from some of the studies discussed above, the difficulty of controlling the inter-particle distance and the mean NP size independently, then makes it difficult to draw definitive conclusions about NP activity.

2.3.3 Stability of nanoparticulate catalysts

In terms of the application of NP catalysts, stability is of paramount importance, as well as the activity and selectivity. Ideally, one would want to study structural changes of real catalysts during operation in a model environment, but in situ structural characterization is challenging. While comparison of the electrochemical surface area before and after a measurement gives some insight into gross structural changes of a catalyst, this is not sufficient to judge unambiguously the mechanism of catalyst degradation and aggregation.

An alternative approach is to measure the structural changes of NPs after 'accelerated aging tests'. Mayrhofer et al. recently reviewed reports of performing such an analysis by a technique called identical location – transmission electron microscopy (IL-TEM) that entailed depositing commercial Pt/C NPs on a TEM grid and subsequently using the grid as an electrode.[230] After an electrochemical aging step performed for several hours, the electrode could be inspected with TEM again. Various types of degradation were identified, namely NP detachment, dissolution and growth. In one case, substantial loss of Pt NPs from the carbon support was observed, which

was attributed to detachment rather than dissolution.[230] For other catalysts however, Pt dissolution was observed, particularly for alloyed NPs such as PtCo NPs. An effect of NP dissolution can be the growth of adjacent NPs, through the Ostwald ripening mechanism,[102, 103] but this has not been observed in IL-TEM measurements, presumably due to the large diffusion distance for Pt ions at the low catalyst loading employed in IL-TEM measurements. While an increase in apparent NP size was found in IL-TEM, this was mainly attributed to agglomeration. Since these effects were often found to occur simultaneously (even on individual carbon support particles) no generally dominant degradation effect could be determined for the Pt NPs. However, the oxidative shrinking of the carbon catalyst support at elevated temperatures and potentials followed by consequent Pt NP migration, was found to be a dominant degradation pathway.

These local results could be extrapolated by measuring the loss of electrochemically active Pt surface area, determined through carbon monoxide stripping voltammetry.[231] However, since the loss of electrochemical surface area can occur via either NP detachment, dissolution, aggregation, or corrosion of the carbon support, electrochemical measurements alone cannot be used to evaluate the exact nature of the catalyst degradation.

Similar degradation measurements were performed in the group of Muller, in which structural information from scanning transmission electron microscopy (STEM) measurements was combined with elemental information through electron energy loss spectroscopy (EELS).[232, 233] After subjecting commercial PtCo alloy NPs to heat treatment, acid leaching, and 30,000 potential cycles in a PEM fuel cell setup, it was reported that NPs grew in a synergetic combination of coalescence and Ostwald ripening. Using EELS, the Co and Pt content could be traced inside individual NPs, revealing that the average PtCo core size did not change, while the Pt skin grew significantly as a result of potential cycling, especially at coalesced particles.[232]

Muller and Abruña et al. used the same setup for an IL-TEM measurement, in which electron tomography was also applied.[233] In this case, the particles were voltammetrically cycled on a carbon-covered Au TEM grid that served as a working electrode in a three-electrode cell, for 30,000 scans between 0.6 and 1.0 V vs RHE. The cyclic voltammograms (CVs) showed a loss in the electrochemically active surface area of ~20% (which was also verified using CO stripping) and a concomitant decrease in the ORR activity. Using STEM, the main cause for the surface area loss could be attributed to NP coalescence, which could be accurately followed using tomography imaging, with no significant change in the PtCo core size. Finally, no obvious degradation

of the carbon support or significant Ostwald ripening of the catalytic NPs was observed in these controlled experiments,[233] in contrast to findings in MEA environments, in which both carbon degradation and NP dissolution has been observed.[234, 235] The authors attributed this contrast to the improved potential control of the three-electrode configuration, limiting the relative mild upper potential limit to 1.0 V, whereas in an MEA the potential can spike up to 1.4 V due to fuel starvation.[235]

2.4 Electrochemistry at preferentially shaped nanoparticles

As highlighted above, the electrochemical performance of metal NPs is typically determined from studies on ensembles of a large number of NPs. However, the inherent dispersion in NP sizes and shapes means that reactivity trends that arise from such studies only reflect the average electrocatalytic behavior of the entire ensemble. Indeed, the overall reactivity of an ensemble may well be dominated by a small fraction of the NPs. These (often poorly reproducible) variations in the dispersion of NP shapes and sizes can make it difficult to compare the findings between different studies. For example, as briefly discussed earlier (Section 2.1.1), contradicting particle size dependencies have been reported for the ORR, as a consequence of difficulties of separating out NP size, shape, coverage, and mass transport effects. In this section, we will discuss an approach to minimize these variations, while still employing large NP ensembles to perform macroscopic measurements, namely the use of NPs with a well-defined (preferential) shape.

Two seminal papers on the preparation of NPs with a preferential shape, through colloidal synthetic methods, were published in 1996, by El-Sayed et al.[236, 237] By tuning the ratio of the Pt precursor and the capping agent (sodium polyacrylate) during the synthesis, mixtures of NPs were obtained with predominantly tetrahedral, cubic, icosahedral or cubo-octrahedral shapes (Figure 2.8). This formation of metastable structures (as opposed to the thermodynamically preferred truncated octahedron shape of a metal NP with a face centered cubic (fcc) lattice) is a result of the anisotropic growth of NPs caused by the preferential adsorption of capping agents and/or other shape-directing agents (such as metal ions) on certain facets during growth, inhibiting the growth of those facets.[238] There have been many subsequent reports, adapting the colloidal synthetic method to fine-tune the shape of metal NPs of various materials; advances in the colloidal synthesis of shape-controlled particles have been extensively reviewed. [131, 239–244]

The first electrochemical study of shape-controlled NPs was published by the Alicante group in 2004.[69] The authors employed Pt NPs with preferential {100} surfaces ('cubic' NPs) to study the oxidation of ammonia.[69] From studies using macroscopic single-crystal electrodes, this reaction is known to be very sensitive to the structure of the surface, with the reaction taking place almost exclusively at Pt(100) sites, and proceeding faster on larger (100) domains.[245] Cubic Pt NPs were found to display a four times higher specific activity than spherical Pt NPs. This result mirrored that found macroscopically, suggesting that single crystal electrodes could be used to predict structural effects in NPs in this case.

There have been numerous subsequent electrocatalytic studies on 'cubic' (predominantly {100} facets, figure 2.8a),[193, 246–255] 'hexagonal' and 'octahedral' (predominantly {111} facets, figure 2.8b)[247, 254] and 'tetrahedral-octahedral' or 'cubo-octahedral' ({111} and {100} facets)[247, 252] NPs of various (fcc) metals for a variety of reactions.[244] Usually, such studies find that the reactivity of preferentially shaped NPs is in qualitative agreement with findings from corresponding single-crystal electrode studies, i.e. 'cubic' NPs show a (typically about 3-10 times) higher specific activity than non-preferentially shaped NPs for reactions that favor (100)-type sites.[193, 247–255]

A notable exception to this finding, in which single-crystal reactivity could not be extrapolated to predict the reactivity of preferentially-shaped NPs, was reported by O'Mullane, Bhargava, et al.[254]. The authors compared the reactivity of spherical (rich in {111} facets), cubic (rich in {100} facets) and prismatic (nominally terminated by {111} facets, but rich in defects) Ag NPs for a number of reactions with preferences for different surface sites (oxide formation and stripping, lead underpotential deposition and stripping, hydrazine oxidation, hydrogen peroxide reduction and formaldehyde oxidation), and found that prismatic NPs were the most active for all these reactions. This finding was explained by the high amount of defects in the prismatic NPs, illustrating that, to study structural effects on the level of a NP, characterizing the amount of defects sites is just as important as tuning the morphology of a NP to expose selected facets.

While colloidal synthesis has proven successful as a means of generating preferentially-shaped NPs terminated by basal plane facets, fundamental studies on macroscopic single crystals have shown that many (electro)catalytic reactions favor low-coordination sites, such as steps, kinks and defects.[5, 44] Therefore, to optimize the reactivity of NPs for such reactions, shape-controlled NPs enclosed by high-index facets would be desirable. The colloidal synthesis of such NPs is not straightforward due

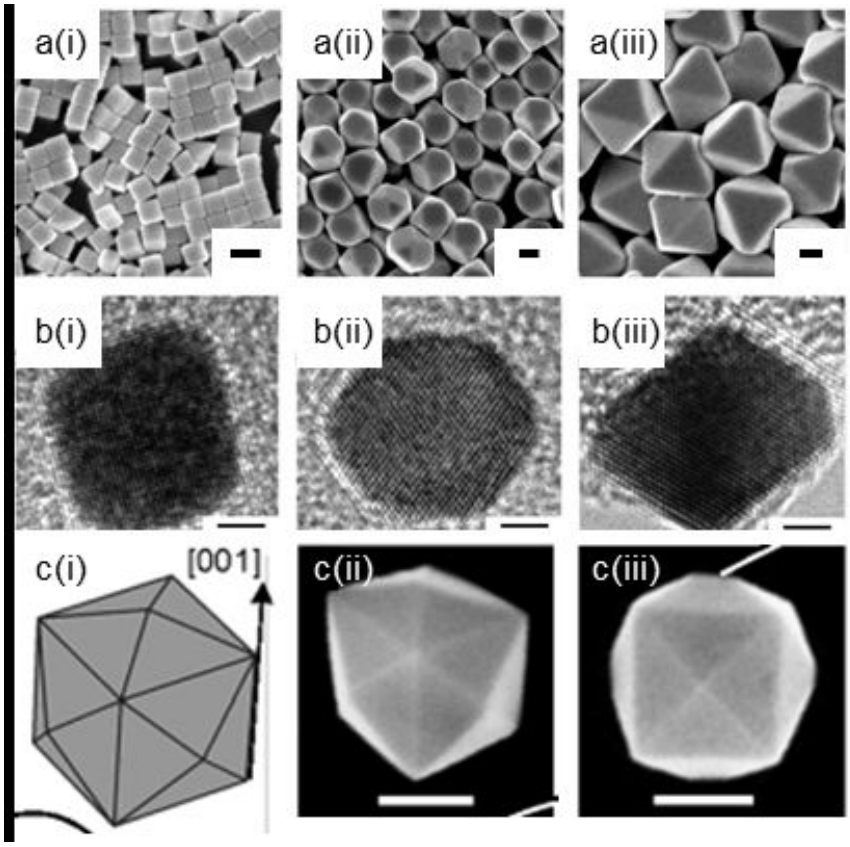

Figure 2.8: Examples of preferentially shaped NPs. (a) SEM images of (i) cubic (bound by {100} facets), (ii) cuboctahedral (bound by {111} and {100} facets) and (iii) octahedral (bound by {111} facets) Ag NPs. Scale bar = 100 nm. (b) High resolution TEM images of a (i) cubic (bound by {100} facets), (ii) cuboctahedral (bound by {111} and {100} facets) and (ii) octahedral (bound by {111} facets) Pt NPs. Scale bar = 2 nm. (c) (i) Geometric model and (ii-iii) SEM images of a tetrahexahedral Pt NP (bound by 24 high-index {hk0} facets, such as 730). Scale bar = 100 nm.(a,b) Adapted from reference [243], ©2011, Wiley-VCH. (c) Adapted from reference [94]. ©2007, American Association for the Advancement of Science.[94].

to the high surface energy of high-index facets, causing them to be eliminated quickly during crystal growth.[256] This problem was overcome by Sun, Wang, et al. who have developed an electrochemical method to prepare NPs terminated by high-index facets.[94, 257]. In this method, 'large' Pt spheres (ca. 750 nm) were electrodeposited on a glassy carbon electrode. Characterization of these spheres revealed that they consisted of small NPs (of a few nanometers). Subjecting these spheres to a square-wave potential treatment (typically 10 Hz, upper and lower potential ~1.20 V and ~–0.20 V vs the saturated calomel electrode, respectively) in an ascorbic acid-containing solution for 10 – 60 minutes caused them to disaggregate into the constituent NPs on the electrode surface, which then underwent dissolution-reprecipitation cycles to form tetrahexahedral NPs of 20 – 220 nm size, bound by 24 {hk0} facets (Figure 2.8c).[94, 257–262] NPs of other preferential shapes, such as concave hexoctahedral (enclosed by {hkl} facets),[263] trapezohedral ({hkk} facets),[262, 263] and nanorods (various {hk0} or {hkk} facets)[263, 264] and metals (Pt,[94, 263, 265] Pd,[260, 263, 264] Fe,[266] PdPt,[259] and PtRh[262]) have similarly been produced by adjusting the synthetic conditions.[256]

NPs prepared by this method have been employed for a variety of electrocatalytic reactions which are known to be promoted by defects and other low-coordination sites (ethanol oxidation on Pt[94, 261, 263] or Pd[260, 263, 264], formic acid oxidation[94] and nitric oxide reduction on Pt,[265] and nitrite reduction on Fe[266]). These particles were typically found to have up to four times higher specific activities than commercially available catalysts, although it should be born in mind that commercial catalyst are optimized for mass activity (see below) and stability rather than specific activity. A further enhancement in specific activity has been demonstrated by modifying the high-index facets of preferentially shaped NPs with a second metal beneficial for a specific reaction, such as Pd for formic acid oxidation[259] or Rh for ethanol oxidation.[262] This can be done either by preparing bimetallic particles during the synthetic procedure, such as PtPd[259] and PtRh[262], or by surface decoration of preformed (Pt) NPs with ad-atoms, such as Bi,[267] Au[268] or Ru.[269]

While the use of tailored, preferentially-shaped NPs (either enclosed by basal planes or by high index facets) is a seemingly straightforward approach to boost the catalytic activity for some reactions, such NPs are quite large (typically > 10 nm for basal plane-faceted NPs and 20-150 nm for high index NPs) compared to commercial catalysts (2-4 nm). Commercial catalysts thus have much better mass activity (current per gram of NP), which is relevant for technological applications, as this ultimately determines the cost of the catalyst material. Ideally, it would be desirable to decrease

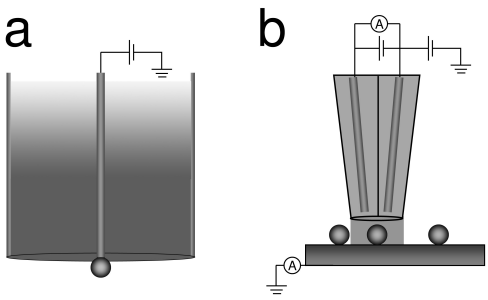

Figure 2.9: Two approaches to study electrochemical reaction at a single NP. (a) A single NP is tethered to a NSE. (quasi reference electrode not shown) (b) The response of a single NP within in ensemble is isolated for investigation. In this example, this is achieved with a scanning electrochemical cell microscopy (SECCM) set-up, discussed in detail in Section 2.5.3.

the size of the preferentially shaped NPs to the 2 – 4 nm regime while maintaining the shape to increase the mass activity, but the synthesis of such NPs is challenging.[258] Furthermore, smaller NPs of this type are relatively unstable due to lower stabilization from the bulk material, and adsorption and reaction of species during electrocatalysis may cause small NPs to change their shape and lose the enhanced activity.

To address the issue of stability of preferentially shaped NPs, Sun et al. have performed a series of molecular dynamics simulations on Pt NPs with various shapes of ca. 5 nm diameter.[270–272] Not surprisingly, it was found that truncated octahedrons showed the highest thermal stability, maintaining their shape up to > 1000 K, whereas preferentially shaped NPs (both basal plane NPs and high index NPs), start to change their overall shape at ~700 K. While this thermal stability seems sufficient for the employment of preferentially shaped NPs in low-temperature electrocatalytic system, the issue of electrochemical stability remains to be investigated. Especially during extended use or repeated start-stop cycles in real applications, the crystalline surface may not be preserved due to oxidation-reduction cycles.[273, 274]

2.5 Measurements of individual metal nanoparticles

The ideal model system is a single NP of well-defined shape and size, studied in an electrochemical cell under potentiostatic control. In this section, we will discuss frontier techniques which have opened up this possibility. Broadly, there are two approaches to study the electroactivity of a single NP (Figure 2.9).

2.5.1 Techniques and Methods

Significant progress has been made on the use of NSEs, which has allowed the measurement of electrochemical processes at electrodes with dimensions down to nanometer dimensions and often with (sub-)pA currents.[32, 275] Fabrication methods for such electrodes were initially based on the encapsulation of sharp (etched) wires, akin to scanning tunneling microscopy (STM) tips, with just the end exposed by sealing in a resist,[276, 277] or by heat sealing in glass.[275, 276, 278, 279] Although very small electrodes can be routinely produced in this fashion, electrodes must be characterized individually before use by a range of techniques in order to determine the actual electrode surface area. Lithographical techniques allow more freedom in the choice of electrode material. Optical lithography was initially employed for the fabrication of UME arrays[280, 281] and electron beam lithography has subsequently been employed to prepare individual NSEs.[282–286]

Alternatively, rather than decreasing the area of an encapsulated electrode material, the contact area of a macroscopic electrode with the electrolyte can be confined to effectively create a NSE. In scanning electrochemical cell microscopy (SECCM),[111, 287–297] an electrolyte droplet at the end of a double-barreled theta capillary, which has been drawn to a very sharp tip, contacts a macroscopic electrode surface. Conventional electrochemical measurements can be made between the exposed electrode surface and (quasi-)reference electrodes contained in the barrels. Furthermore, this configuration also allows two-dimensional maps of localized electrode reactivity to be obtained, as discussed in detail in Section 2.5.3. This technique improves on related microdroplet techniques in terms of the spatial resolution attainable and information content of experimental data.[298–302]

Ideally, to characterize the electrocatalytic activity of metal NPs, one should aim to probe them individually, to determine the impact of particle size and shape on catalytic performance directly and unambiguously. However, the direct characterization of the surface of a single NP is extremely challenging. For example, noble metal electrodes are often characterized by measuring the formation and stripping of an oxide monolayer (see Section 2.2.5), with a charge of approximately 400 μC cm^{-2}.[192] For NPs with radii of 10 nm and smaller, this corresponds to ca. 10^{-15} C or less. Measuring such small charges requires very high accuracy current amplifiers with a fast response time, which is a fundamentally difficult combination, although promising results have been reported for state-of-the art integrated amplifier-electrode systems.[303, 304] On the other hand, diffusive processes, such as outer-sphere reactions and some electrocatalytic processes (e.g. hydrogen evolution and oxidation, hydrazine oxidation,

oxygen reduction) are more readily measurable, as will be shown below. The limiting current at an isolated catalyst NP (with diffusion as the sole mass transport mode) is manifested in a steady state current ($I_s s$):[305]

$$I_{ss} = nFAkTC = nFA\chi DC \tag{2.4}$$

where F is the Faraday constant, n the number of electrons transferred during the reaction, C the bulk concentration of the reactant, A the surface area of the particle, and kT the mass transport coefficient, which is the product of a geometry factor (χ) specific to the NP arrangement, and the diffusion coefficient of the reactant species (D). χ is $ln(2)/r$ for a sphere on an infinite plane,[306] $1/r$ for a perfect (hemi-)sphere, and $4/\pi r$ for an inlaid disk, where r is the radius of the (effective) electrode (NP).[305] Taking the four electron ORR in an oxygen-saturated aqueous solution (ca. room temperature) as an example (C $\approx$ 1 mM, $D = 1.8 \times 10^5 cm^2 s^-1$), a 5 nm radius spherical particle on a plane gives a steady-state current of ~15 pA, which is well within the capabilities of commercial current amplifiers.

2.5.2 Immobilized nanoparticle measurements

An obvious method to measure the electrocatalytic activity of an individual NP, is to immobilize it onto a nanoscale support electrode, ensuring that the NP response can be measured, with a low electrochemical background current. This approach is exemplified by the work of Kucernak et al.,[38, 49, 307, 308] who electrodeposited a single Pt NP on (the end of) a carbon nanofiber (Figure 2.10), a support showing negligible Faradaic activity over a wide range of potentials.[307] The nanofiber was first sealed in a layer of electrophoretic paint with only the apex left uncoated, to minimize the conductive area. Subsequently, Pt was electrodeposited using potential pulses of well-defined duration, with the pulse length correlating to the final particle radius.[38] In this way, the influence of NP radius was investigated for the kinetics of the ORR and HOR.[49, 308] For the ORR (in 0.1 M H_2SO_4), an effective number of electrons, n_{eff}, of 3.5 was found in the diffusion-limited regime for NPs smaller than 100 nm. This number was inferred from the diffusion-limited current using equation (2.4), for which χ was determined using the HOR (n=2) on the NP electrode, and D obtained from UME measurements.

The effective number of electrons transferred per O_2 molecule depends on the relative yields of hydrogen peroxide (2 electrons per O_2 molecule) and water (4 electrons per O_2 molecule). A transfer of only 3.5 electrons per oxygen molecule implies that 25

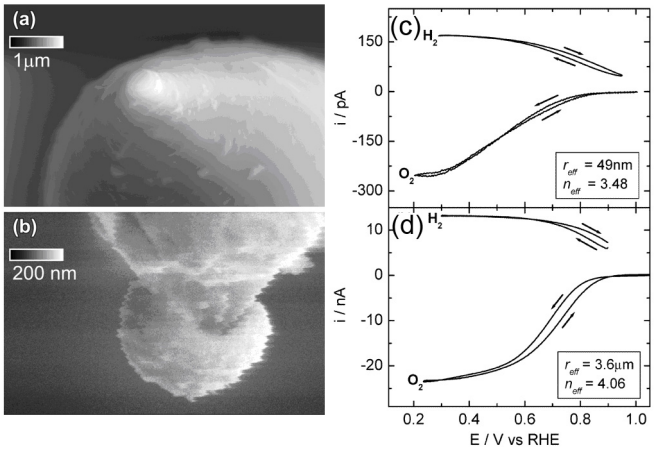

Figure 2.10: A Pt NP electrodeposited at the apex of a carbon tip (a,b). The kinetics of ORR and HOR are a function of the radius of the particle as evidenced for two different radii (c and d). Adapted from references [38] (©2003, American Chemical Society) and [308] (©2004, American Chemical Society).

% of the oxygen is converted to hydrogen peroxide without reacting further to water (see Figure 2.2, Section 2.1.1). For particles smaller than 100 nm the mass transport ($kT > 2$ cm s^{-1}) is so fast that some of the H_2O_2 produced escapes the electrode vicinity and is transported into the bulk electrolyte. These findings are consistent with the proposed mechanism on the role of mass transport in NP ensembles outlined in Section 2.3, at least qualitatively. It should be noted that these measurements were conducted without detection of hydrogen peroxide, which would have underpinned the mechanistic interpretation of the data.

The extremely fast mass transport to and from individual NPs allows the study of reaction mechanisms in potential regimes where the current is normally dominated by diffusion limitation (e.g. in rotating disk electrode measurements). Thus, for particles smaller than 50 nm (kT > 4 cm s^{-1}), no clear mass-transport limited current was observed. It was reasoned that at these high mass-transport conditions, significant kinetic limitations pushed the ORR into the potential domain where hydrogen adsorbs on the Pt surface (H_{UPD}).

In the HOR, the high mass transport conditions of the experiment allowed the observation of an extra current plateau in the H_{UPD}. Fitting the CVs by a kinetic model, the Tafel-Volmer mechanism was found to be the dominant mechanism rather than the Heyrovsky-Volmer mechanism, as discussed in the Introduction (Section 2.1.1).[49]

Individually electrodeposited particles were also used in a study by Bard et al.,[309] where a carbon fiber, biased at the Pt electrodeposition potential was covered with a film of electrophoretic paint containing pinholes. As the fiber was gradually immersed into a solution containing Pt(II) ions, a cascade of reduction transients was measured as a function of the tip immersion depth, indicating Pt deposition at the pinholes. Subsequently, slow immersion into a fresh electrolyte containing Fe_3^+ (enhanced reduction kinetics on Pt with respect to C) showed discrete increases in the reduction current as the freshly generated Pt NPs gradually came into contact with the solution, so that the contributions of the different particles were separated in time and space.

Poor control over NP shape is a major disadvantage (Section 2.2.1) of using electrodeposition to immobilize a particle on an electrode, and particle stability on the support has been reported to be problematic.[309] To circumvent these problems, single colloidal NPs with fine-tuned shape and size can be attached to a NSE with radius equal to or smaller than the NP size from a dilute colloidal solution.[154, 168, 310] However, it is not trivial to produce, handle and characterize NSEs with radii below 10 nm,[311–314] and there is a restriction on the choice of electrode materials.[315]

Zhang and co-workers immobilized a single Au NP on an oxidized Pt NSE through a silane linker terminated with an amino group. An individual NP was found to adhere to the modified electrode (in TEM analysis), when it was immersed in a solution containing NPs.[154] Similarly, Sun et al. reported the attachment of a single Pt NP on a Au NSE through an alkanethiol linker.[168, 312] In another experiment, the surface of a Pt NSE was not modified, but cycled voltammetrically in a solution containing Au colloid. When a reduction current was observed in the CV this was interpreted as the arrival of a single Au NP.[310] Electrochemical analysis of these individual probes included the deposition of Cu monolayers[154] and the measurement of Au blank CVs in sulfuric acid.[154, 310] Both of these methods can be employed to determine the electrochemically active surface area of an electrode,[192] but as mentioned earlier, such surface electrode measurements are challenging, and in these particular studies the surface area was significantly overestimated compared to ex situ electron microscopy measurements. The authors tentatively rationalized this by suggesting that the bulk Au atoms were also oxidized in addition to the surface atoms, leading to Au reduction charges higher than expected.[310] Unexpectedly, ORR measurements revealed a lower overpotential for Au NPs compared to the bare Pt disk UME, but a much smaller diffusion-limited current, suggesting that the Au NP was not participating fully in the reaction.[154] Regardless of these inconsistencies, these experiments indicate the possibility of immobilizing single catalyst NPs and studying their reactivity and we

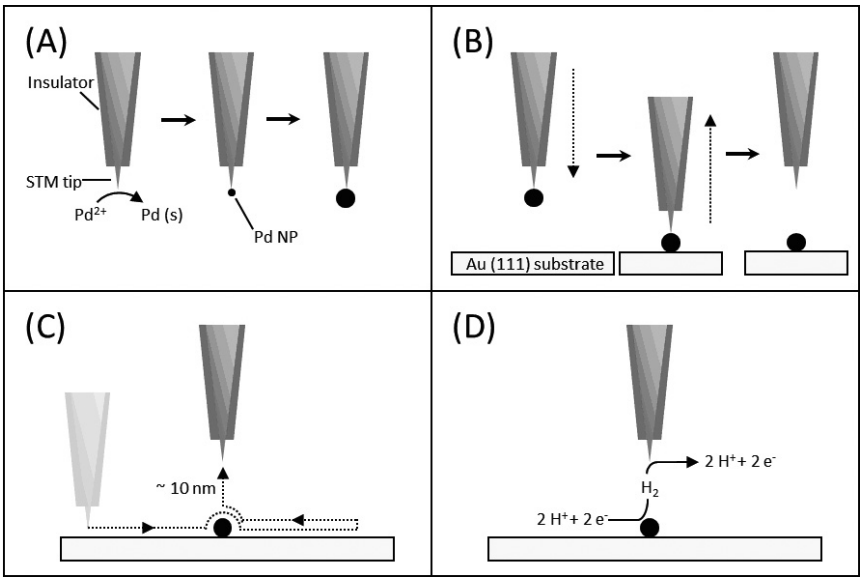

Figure 2.11: Schematic representation of the single NP experiment by Stimming et al.[54] Through electrodeposition, a Pd NP is formed at the tip of an STM probe (a), which is then deposited onto an Au surface (b). The surface-immobilized NP is imaged with the tip (c) and the tip is then moved back 10 nm and used in 'collector-mode' (i.e. as an SECM tip) to detect H_2 produced by electrocatalysis at the NP (d). Adapted from reference [218]. ©2012, Cambridge University Press.

anticipate much further development in this field.

Rather than immobilizing the NP on a very small electrode, one might choose to deposit particles at a known location on a macroscopic electrode using the high spatial resolution afforded by scanning probe techniques, such as scanning tunneling microscopy (STM), as shown in Figure 2.11. Once the NP is on the macroscopic electrode and located by the STM tip, it is biased to promote an electrochemical process of interest, and the probe tip (moved back by ~10 nm) then serves as a collector electrode to detect any generated products in an SECM-type configuration. In this way, the HER kinetics at a single Pd particle was studied by applying different potential pulses to the substrate and measuring the collector current.[54] The reaction rates were found to decrease with increasing NP height (total amount of Pd layers). In fact, NPs consisting of less than 5 Pd layers were found to be orders of magnitude more reactive than those with more layers. This effect was modeled using density functional theory calculations, and it was interpreted as arising from the strain induced on the Pd NP due to the lattice mismatch with the underlying Au(111) substrate. The strain increases the average

Pd-Pd distance, on which the HER reactivity is primarily dependant.[316] While this method presents an elegant way to study size effects on electrocatalysis at a single NP, the interpretation of the experimental results is not straightforward and has led to considerable discussion.[317] Nonetheless, this type of measurement demonstrates the insights offered by SECM-type measurements using ultrasmall probes.

2.5.3 Nanoparticle landings

It is not necessary to pre-immobilize NPs on an electrode as in the approach described in Section 2.5.1; their arrival at electrodes from a (dilute) colloidal solution may also be detected electrochemically. When an electrocatalytically inert UME is immersed into a solution containing both a reactant and a catalyst NP, on which that reactant can be turned over, a current signal is measured whenever a NP is polarized by colliding with the UME. This approach can be traced to the studies of Heyrovsky et al. who showed that the reduction of polydisperse ceramic semiconductor NP colloids contributed to the cyclic voltammetry of a Hg drop electrode by a summation of cathodic steps that had an onset potential dependent on the particle size.[318–321] In a later study on the interaction between metallic NP colloids and an Hg electrode, it was found that the cathodic waves measured consisted of discrete contributions from the reduction of the oxidized NPs arriving at the electrode.[322] It has also been demonstrated that the faradaic current at an UME performing a redox reaction decreased in discrete steps upon the addition of insulator microparticles. Optical microscopy indicated that the blocking of the electrode by these particles was the cause for the diminished current.[323, 324]

The first detection of NPs through electrocatalytic amplification (Figure 2.12) was demonstrated by the Bard group, using a carbon UME with Pt NPs in solution, held at a potential at which hydrogen evolution would occur on Pt but not on carbon. Current spikes were detected with a frequency that could be roughly correlated with the expected diffusional flux of NPs toward the electrode surface (vide infra).[306] This type of experiment has since been reproduced by several research groups for a number of combinations of the electrode material, the NP material and the reactant molecule, as well as variations in the experimental set-up and coupling with other techniques (see Table 1). Broadly speaking, two distinct types of reactivity have been observed: a cumulative cascade of current steps (‘a staircase’) and a series of transiently decaying current jumps (‘spikes’). A current staircase is expected for the landing of NPs on an electrode that catalyze a reaction continuously. Current spikes are observed when NPs continuously arrive at a surface, but their reactivity is finite.

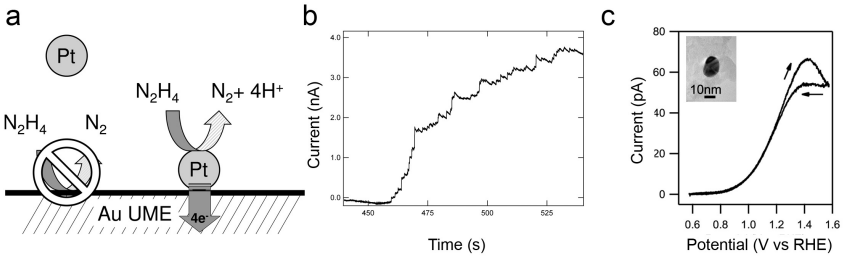

Figure 2.12: An inert UME is in a solution containing an electrocatalytic reactant and catalyst NPs; as NPs impact the surface they convert the reactant and a current is measured (a). If the NPs stick to the surface, the current contribution is continuous, resulting in a staircase-type current-time plot (b), as at an Au UME in presence of Pt NPs in a hydrazine-containing solution. (c) Cyclic voltammogram (200 mV s^{-1}) for the oxidation of 2 mM hydrazine at a single Au NP (shown in inset) on a TEM grid electrode. Adapted from references [327] (©2013, American Chemical Society) and [293] (©2012, American Chemical Society.)

Electrocatalytic current step heights measured when NPs land on an electrode can provide an insight into the particle size, through equation (2.4. This is well-illustrated by several studies of the oxidation of hydrazine at Pt NPs landing on Au UMEs,[293, 325–328] where the landing frequency and current step height distributions were in reasonable agreement with the concentration and size distribution of the NPs as determined by other methods, such as TEM.[325] However, it should be noted that the size of NPs can only be determined accurately from diffusion-limited reactions if the diffusion coefficient of the reactant molecule is known or can be determined with a high degree of certainty. This may appear to be a trivial and obvious point, but is particularly troublesome for hydrazine, a popular reactant for this type of experiment for which the reported diffusion coefficients show a significant spread, ranging from ~10^{-8} to ~10^{-3} cm^2 s^{-1}, with typical values between 0.6 – 2.0 $\times$ 10^{-5} cm^2 s^{-1}.[55, 56, 329–332] This has a corresponding impact on the use of amperometry to determine NP size, considering that the limiting current depends linearly on the diffusion coefficient (equation 2.4).

To confirm that Pt NPs catalyze the hydrazine oxidation, Bard et al. studied the effect of treating the particles or the UME with self-assembled monolayers (SAMs).[326] When an UME was treated with an alkanethiol with a chain length up to 12 methylene units, landings of as prepared (citrate-capped) Pt NPs could still be detected, but the magnitude of the current step per landing decreased with increasing chain length. The authors suggested this to be due to the suppression of electron tunneling from the

NP through the SAM to the UME,[326] although this would appear to be contradict to the Chazalviel-Allongue model (see Section 2.2.3).[183] Conversely, if the NPs were capped with an alkanethiol SAM, the ability to detect their landing was significantly reduced when the carbon-chain length was increased; even for the shortest chain length of three carbons a much lower landing frequency was detected. Capping the NPs with other stabilizing molecules typically used in NP synthesis, such as polyvinylpyridine (PVP) and cetyltrimethylammonium bromide (CTAB) resulted in a similar loss in the ability to detect collisions. These findings were rationalized as follows: hydrazine oxidation requires certain catalytic surface sites on the NP, which are blocked by strong capping agents, whereas ET from the NP to the UME is governed by electron tunneling (and is thus relatively insensitive to the nature of the capping agent)[326] Aside from proving the proposed mechanism of detection of NP landing, this method could also be used to evaluate charge-transfer between a NP and electrode through organic molecule SAMs.

The inability to detect NPs after changing the NP capping is one reason why the majority of successful NP landing experiments makes use of citrate-capped NPs. The interaction between citrate and the NP metal surface is such that the surface reactivity is not hindered significantly, while electrostatic repulsion between NPs in solution limits aggregation. The adsorption strength of citrate on Au surfaces is comparable to that of anions such as sulfate,[333, 334] which is known to diminish, but not block, catalytic reactivity,[44] while organic molecules such as PVP and CTAB have a stronger surface interaction and tend to inhibit catalytic activity more significantly.[184]

Rather than using conventional glass-sealed UMEs, Kleijn et al. employed lithography to fabricate Au UMEs as the support electrode for NP landings.[327] They found that the landing frequency for Pt NPs (using hydrazine or hydrogen as the reactant) was much lower than expected and that the distribution of current step magnitudes from a series of landings showed significant tailing at higher current values.[327] Both the lower landing frequency and the observation of larger currents could indicate a reduced effective NP concentration, which was attributed to the aggregation of NPs in solution. Aggregated NPs were observed by scanning electron microscopy (SEM) on the support electrode after a landing experiment. However, when NPs were landed in absence of hydrazine or hydrogen, no aggregates were detected on the UME, demonstrating that NPs in solution can aggregate by interaction with the reactants added for NP detection. It was proposed that the weakly bound citrate molecules were displaced by the hydrazine or hydrogen and that the diminished electrostatic repulsion resulted in aggregated NPs.

An alternative platform to prepare an electrode for NP landing experiments is by using SECCM, as recently introduced by Unwin and co-workers,[293] A SECCM probe, containing an electrolyte solution with Au NP colloids, was moved slowly towards the working electrode until the meniscus at the end of the pipette made contact with the conductive substrate, thereby forming a nanoscopic electrochemical cell to perform NP landing experiments. Compared to the landing experiment describe above, that employ preformed UMEs, this approach offers a several key advantages. First, a wide range of materials can be used for the support electrode, as no traditional UME manufacture is required. Second, the cell can be made and broken at will on a millisecond time-scale at specified locations. Finally, ultrasmall electrode areas can readily be achieved by employing pipettes with smaller diameters, offering a significant decrease in background current.

The high sensitivity of this approach was demonstrated by measuring Au NP landing experiments on highly oriented pyrolytic graphite, a carbon support with very low background currents for which it is unfeasible to prepare a UME or NSE by conventional methods. The landing of Au NPs was detected throughout various potentials for the ORR and HER processes, including potentials at which the magnitude of the individual current steps was less than 1 pA. The versatility in the choice of substrate was further emphasized by landing Au NPs onto the carbon foil of a TEM grid which was connected as a working electrode, using the oxidation of hydrazine as a probe reaction. After the first current step (indicating the arrival of a single NP at the TEM grid), the tip was retracted and the grid was characterized by TEM, allowing a correlation to be made between the current magnitude of the landing step and the NP size. An estimation of NP sizes from the current responses, using equation 2.4 provided values that were in good agreement with the actual NP sizes.[306] Additionally, a cyclic voltammogram of hydrazine oxidation on a single gold nanoparticle could be measured, as shown in Figure 2.12c. This approach has considerable promise for structure-reactivity measurements at the single NP level.

Bard and co-workers have diversified combinations of NP metals and electrocatalytic reactants that can be studied by NP landing. Thus, Au NPs were detected through the oxidation of borohydride, which can be suppressed on Pt UMEs that have been pre-oxidized. These collision measurements showed spiked responses, suggesting that the NPs either desorbed from the electrode surface or stayed in place, but became deactivated.[335] Similar results were found for the detection of iridium oxide (IrO_x) NPs using the OER; since IrO_x is more active than Pt for the OER, current spikes could be observed at a potential just below the onset of OER current on Pt

UMEs.[336] To gain additional insight into the current decay transient observed for IrO_x NPs, the landing detection was performed in an SECM configuration where a macroscopic surface (2 mm diameter Pt disk) and a Pt SECM tip (5 µm radius) were held in close proximity (i.e. 50 µm separation) and biased at the same potential (0.8 V vs Ag/AgCl).[337] NP landings were monitored at the SECM tip while the macroscopic disk acted as a NP sink (shielding experiment). The landing frequency of IrO_x NPs was seen to decrease as a function of time, due to NP adsorption at the macroscopic electrode. It was thus deduced that the current-time transient for the OER at IrO_x NPs was due to irreversible sticking and subsequent deactivation rather than to an intermittent contact between the NP and the collector UME.

The Compton group[338] has adopted the NP landing methodology to measure the size distribution and concentration of NPs in solution, through a method coined 'anodic particle coulometry' (APC).[339] When a NP contacts a glassy carbon UME that is held at a potential to promote electrodissolution of the metallic NP to its constituent ions, an anodic current-time transient is measured. By measuring the charge transferred in the transient, the amount of atoms per NP can be determined, and the original particle size distribution can be derived if the average particle shape is known.

landing frequency (in $10^4 s^{-1} pM^{-1} cm^{-2}$)	Reaction	Response type	NP material / size	UME material / radius	Reference
8.0	HER	Spike	Pt / 4 nm	C / 4 µm	[306]
2.4 – 4.0	HZ Ox	Staircase	Pt / 4 nm	Au / 5 µm	[325]
1.3 – 0.71	$NaBH_4$ Ox	Spike	Au / 14 nm	PtO / 5 µm	[335]
8.9	OER	Spike	IrO_x / 28 nm	Pt / 5 µm	[336]
0.0071	HZ Ox	Staircase	Pt / 4 nm	Au* / 2000 μm^2	[327]
4.0	Red Ox	Staircase	Au / 20 nm	C† / 0.5 µm	[293]
3.9	Ag NP Ox	Spike	Ag / 20-50 nm	C / 11 µm	[338]
2.4	Th UPD	Spike	Ag / 45 nm	C / 11 µm	[340]
3.2	Cd deposition	Spike	Ag / 45 nm	C / 11 µm	[341]
4.1	Ag NP Ox	Spike	Ag/14,29,45nm	C / 11 µm	[342]
5.2	H_2O_2 Red.	Spike	Ag / 14 nm	C / 5 µm	[343]
2.6	NTP Ox	Spike	Ag / 45 nm	C / 11 µm	[344]
0.33 – 0.49	HZ Ox	Spike	Pt / 4, 12, 22nm	Hg@Pt/12.5µm	[328]
0.25	HZ Ox#	Spike	Pt / 16 nm	Au 5 µm	[345]

Table 2.1: Comparison of landing frequencies of NPs measured in different reports. Measurements were made at disk-shaped UMES, except where *a rectangular, lithographical electrode was used and †measurements performed in a (SECCM) droplet cell setup. #Detection by measuring change in the open-circuit potential.

The formation by electrodeposition of a metal shell on a NP upon impact has also

been reported: for impacting Ag NPs, current peaks were measured at potentials below the Ag oxidation potential, in the presence of ionic thallium[340] or cadmium.[341] The integrated charge passed during each spike could be related to the amount of monolayers of metal deposited on the NP. Depending on the applied potential and the depositing metal, both the underpotential deposition (UPD) and the bulk deposition of metals could be achieved. In another report, the oxidation of adsorbed molecular monolayers from metal NPs was shown to be measurable.[344, 346]

The landing of Pt NPs at a Hg-modified Pt UME has also been reported by Stevenson et al.[328] Since Hg is a very inert electrode material for electrocatalysis, it is an interesting candidate to use for the electrocatalytic detection of NP landings, as illustrated earlier in the pioneering studies of Heyrovsky et al. on NP detection.[318–321] First, a thin film of Hg was formed on the Pt UME by electrodeposition. The Pt NP landings were then measured by the oxidation of hydrazine, which appeared as spikes rather than a staircase response. It was argued that the Hg thin film passivating the Pt UME amalgamates with the Pt NPs, thereby deactivating them.

Quantitative analysis of nanoparticle landing measurements

Attempts have been made to correlate the NP landing frequency to diffusion-based mass transport of particles towards the collector electrode, which is assumed to occur when a NP concentration gradient builds up near the electrode which acts as a sink for NPs.[347–350] The landing frequency is then expected to scale with the UME radius, from the diffusion limited flux function for in inlaid microdisk geometry (analogous to equation 2.4):

$$f_N P = D_{NP} C_{NP} r_{UME} \tag{2.5}$$

where f_{NP} is the landing frequency, D_{NP} and C_{NP} are the NP diffusion coefficient and NP bulk concentration and r_{UME} is the disk UME radius. The NP diffusion coefficient can be estimated from the Stokes-Einstein equation:

$$D = \frac{k_B T}{6\pi\eta r_{NP}} \tag{2.6}$$

where η is the dynamic viscosity of the solution (η ~ 8.90 $\times$ 10^{-4} Pa s for dilute aqueous solutions) , r_{NP} is the NP radius, k_B is the Boltzmann constant (k_B = 1.381 $\times$ 10^{-23} J K^{-1}), and T is the temperature. However, landing frequencies predicted from the simple diffusion model of equation 2.5, consistently overestimate the landing frequency when compared to experimental data in Table 1.

Experimentally, the landing frequency has been shown to correlate with the radius of the electrode,[347] the concentration of NPs,[325, 328, 338, 347] and the viscosity of the solution.[347] However, the NP size should also influence the landing frequency as the diffusion coefficient depends reciprocally on the NP radius, rNP, through equation 2.6. Therefore, as the NP size is increased, the NP diffusion rate and consequentially the NP-UME collision frequency should decrease. For the NP sizes reported in the literature, with radii in the range 2 to 25 nm (as summarized in Table 1), an order of magnitude difference in the diffusion coefficient is expected. However, such a correlation is not evident even though many different NP sizes have been studied to determine the influence of the NP radius on the magnitude of the current response.[325, 328, 338]

The apparent overestimation of landing frequency when using equation 2.5 suggests that this equation does not model real NP landings particularly well, and that a more detailed model should be formulated. Attempts at modifying the original model have been made, for instance by the introduction of a factor that takes into account that not every collision results in NP sticking, and not every sticking NP might yield a measureable response.[347] Another possible explanation for the diminished collision frequency could be due to NP collisions on the insulating sheath surrounding the inlaid metal electrode. The area of the sheath is typically several orders of magnitude larger than that of the collector electrode, and if the sticking probability of NPs onto the sheath was finite, it could act as a NP sink and effectively shield the collector electrode.

Another issue in the quantitative description of NP collisions is that the shape of the current response measured does not always match the expected behavior. For instance, for the HER on Ag[338] or Pt[306] NPs on GC UMEs, current spikes are detected rather than the staircase expected of NPs at which the electrocatalytic reaction is continuous. On other carbon substrates (HOPG and TEM grid C foil),[293] a staircase-type current increase has been reported for the hydrazine oxidation and ORR, indicating cumulative sticking of NPs on the electrode surface. Moreover, for the oxidation of NaBH4 on Au NPs[335] and oxygen evolution on IrO_x NPs[336] at passivated Pt electrodes, current spikes are detected instead of a staircase response. Also, the detection of Pt and Au NPs on boron-doped diamond UMEs via the hydrazine oxidation reaction showed a staircase response for Au NPs, and current spikes for Pt NPs.[351]

Interestingly, landing frequencies obtained with the different characteristic current responses (i.e. spike or the staircase characteristic), are very similar, even though it has been suggested that the spike response corresponds to a non-sticking interaction with the electrode. It was reasoned by Bard et al. that the interval in which a non-

sticking NP is in close proximity to the electrode to experience multiple collisions is too short to be resolved using conventional electrochemical techniques.[347] Therefore, the UME-NP interactions are 'bunched' into a common current response. The frequency of the current response is then equivalent to the diffusion of the NPs towards the electrode and the landing frequency is that of sticking particles. Thus, the landing frequency cannot be used to distinguish between different interactions of the NP and the UME.

Based solely on the electrochemical NP landing detection it is difficult to differentiate between sticking followed by deactivation and a transient, 'bouncing' interaction, since the transient electrochemical signal and the landing frequency alone do not contain enough information to make this distinction. The staircase responses measured in electrocatalytic NP sticking experiments also show a decay on a long (i.e. seconds) timescale.[325, 327] The charging time of the double-layer, or the electrical time constant of the measurement system are much smaller than this and do not explain the current decay. Physical effects, such as the contamination of the catalytic surface by trace amounts of poisonous species in the electrolyte could cause the transient effect, by deactivating the NP. In the groups of Koper and Unwin, electron microscopy was used to show that, after landing was detected via a staircase current, NPs remained on the electrode after the detection measurement.[293, 327] The current spikes observed by Bard et al. during the landing of IrO_x NPs were shown to be due to NP deactivation, rather than desorption, by using SECM,[337] although ex situ electron microscopy would provide a more definitive conclusion for such studies.

2.5.4 Measurements at the single nanoparticle-level within nanoparticle ensembles

Recently, there has been a renewed impetus to study NP ensembles at the level of a single NP with the development of novel frontier techniques. One such technique is SECCM, discussed briefly above and shown in more detail in Figure 2.13a. SECCM employs a dual-barrel (theta) pipette as a probe, pulled to a sharp point with a laser puller to the desired dimensions (~100 nm – 50 µm). Ultimately, the dimensions of the pipette determine the spatial resolution of SECCM. After rendering the outer wall of the pipette hydrophobic, both barrels are filled with an electrolyte solution of interest, and a quasi-reference counter electrode is inserted into each barrel. A small potential bias is applied between the two quasi-reference counter electrodes (QRCEs) to induce an ionic conductance current across the electrolyte meniscus at the end of the tip. The potentials of the QRCEs can be floated with respect to ground, while maintaining the

potential bias between them, to set the effective potential at the substrate, which is held at ground.

To obtain two-dimensional maps of substrate reactivity, the electrolyte meniscus at the end of the pipette is brought into contact with the substrate. This is aided by a small oscillation (typically 10-30 nm) applied to the pipette in the direction perpendicular to the substrate, that causes a periodic deformation of the meniscus and gives rise to an alternating current (ac) component to the ionic conductance current. The ac magnitude is strongly sensitive to the distance between the end of the pipet and the substrate, and can be used as a feedback parameter to maintain a constant separation while scanning across the surface, producing two-dimensional maps of surface activity and surface topography simultaneously.

By employing pipettes of a size smaller than the average interparticle distance, Lai et al. studied electrocatalytic Pt NPs within an ensemble directly with SECCM (Figure 2.13).[111] The Pt NPs were prepared by electrodeposition on a single, isolated carbon nanotube supported on a silicon-silicon oxide wafer. The carbon nanotube not only served as a template for electrodeposition, but also as a nanoscopic wire to electrically connect the NPs (Figure 2.13b). Typical maps of surface activity obtained with SECCM are shown in Figure 2.13c. Comparing the activity maps with the AFM image shows there is an excellent correspondence between the electrocatalytically active regions and the location of the individual NPs. SECCM maps were obtained at various potentials, corresponding to surface oxidation processes as well the ORR and the HER. By measuring the potential-dependent electrocatalytic response of individual NPs and correlating it with the size and structure obtained with AFM and SEM, resulted in several notable findings. First, the reactivity of indivual NPs was highly non-uniform, with subtle changes in NP size and shape leading to significant changes in activity. Furthermore, different NPs displayed different current-potential profiles, even though the average current over the total ensemble yielded an 'expected' potential-dependent current profile. In some cases, NPs that were active for the ORR showed no activity towards the HER. Finally, the study also demonstrated the very high sensitivity of this frontier technique, being able to measure currents of ca. 10 fA over a 40 ms measuring time, corresponding to the reduction of ~600 O_2 molecules (assuming a 4-electron transfer process).

A recent report demonstrates the ability of a combined AFM-SECM approach to measure electrochemistry at individual nanoparticles.[352] In their work, Demaille et al. dispersed Au NPs on a substrate covered with an alkanethiol SAM, and modified the NPs with a redox-labeled ferrocene-polyethylene glycole capping agent (Fc-PEG).

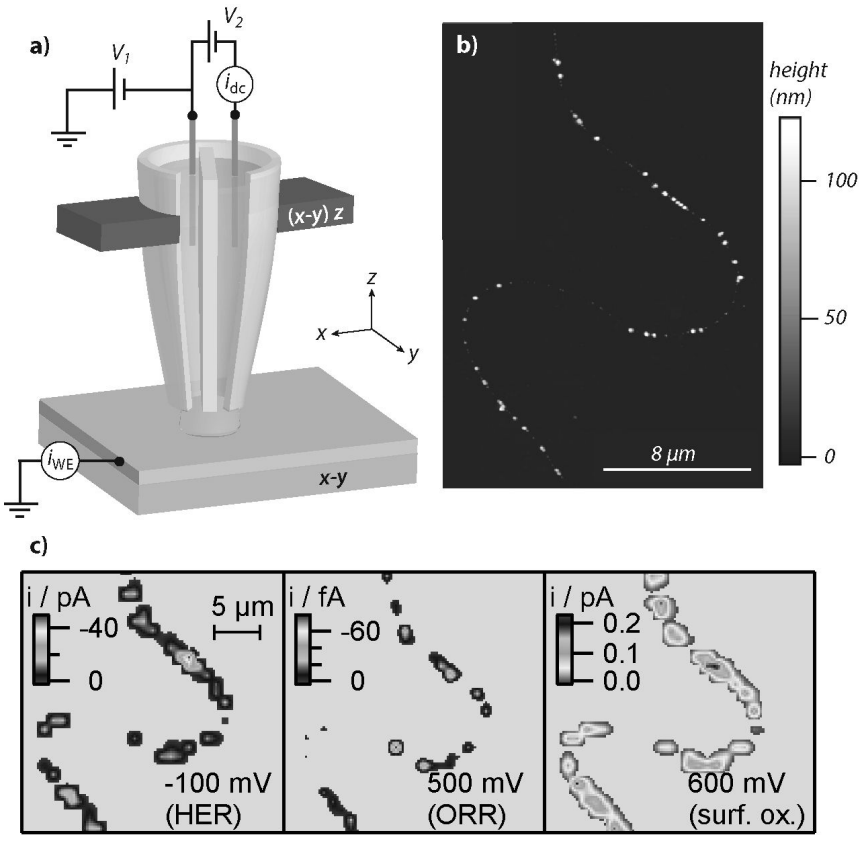

Figure 2.13: (a) Schematic of a scanning electrochemical cell microscopy (SECCM) set-up. Adapted from ref [297]. (b) AFM image of Pt NPs deposited on a single carbon nanotube. (c) SECCM images of the same area as panel (b) at -100 mV (HER), 500 mV (ORR) and 600 mV (surface oxidation) vs Pd-H_2, respectively. Adapted from reference [111]. ©2011, American Chemical Society.

A conductive AFM tip of ~100 nm radius was used to turn over the redox-strands shrouding the NPs and measure the corresponding current response. A variance in NP activity was detected, as only about 80% of the NPs measured by AFM in topography mode generated a measurable SECM current. Demaille et al. attributed this to the unsuccessful grafting of the Fc-PEG at possibly contaminated NPs, as in a separate conductive AFM experiment they show that approximately 90% of the NPs were in fact electronically coupled to the substrate electrode. It should be noted that the SECM currents were rather small compared to the background signal and significant signal processing and digital filtering was needed to extract the SECM currents (~300 fA).

Another recent technique to study individual NPs within an array employs an optical method based on surface plasmon resonance (SPR).[353] SPR is rather sensitive to refractive index variations near a metal surface,[354] and refractive indexes change when reactants are converted at an electrode surface.[355] This method was applied to detect hydrogen evolution at an array of NPs. A CV was recorded on the entire ensemble while following localized changes in SPR, which could be related to single NPs. Apparent CVs for individual NPs could be reconstructed using the potential-dependent SPR changes of the NPs.[353] For 80 nm diameter Pt NPs, a wide variability from one NP to the next in the HER current was found at a potential of -0.2V vs RHE, which is similar to the changes in activity observed in the studies by Lai et al. highlighted above.[111]

Electrochemical strain microscopy is also emerging as an insightful technique for probing electrocatalytic activity on the nanoscale in certain environments. This technique can be used to detect catalytic effects of individual NPs in a model solid-oxide fuel cell environment.[356] In this study, a platinized tip of an AFM was placed in contact with a surface that conducted oxygen ions (yttrium-stabilized zirconia; YSZ), in ambient air. A potential bias was then applied that resulted in the ORR/OER reaction at the tip, leading to a diffusion of oxygen vacancies in the YSZ lattice towards the surface. The movement of vacancies resulted in strain that could be detected by the probe as surface deformations on the pm level. When the tip was on or near a catalyst NP, the applied bias also affected the NP, resulting in enhanced ORR/OER. In this way, an electrochemical map was made of Pt nanoislands evaporated onto a YSZ support, using the ORR/OER system, on which the Pt areas had the highest ORR/OER activity. So far, due to the ultralocal nature of the probe (i.e. the tip is much smaller than the nanoparticles), no quantitative information regarding the shape and size dependence of the catalytic activity could be obtained, although these studies further highlight how local probes have considerable prospects for unraveling the activity of complex NP

electrocatalysts.

2.6 Conclusions and Outlook

In this chapter, we have highlighted and discussed recent reports on the electrochemistry of NPs, with particular attention given to electrocatalytic processes which are among the most widely studied. While a wide range of NP configurations has been considered, from extensive ensembles to individual NPs, the focus has been on studies which provide enhanced (quantitative) information on NP activity through investigations characterized by well-defined mass transport and/or making use of NPs of highly defined architecture, or where structure can be measured and related to activity at the single NP level.

Much progress has been made in controlling NP shape and size, particularly in the colloidal synthesis of NPs. Many different shapes can be made reliably and these shape-tailored NPs typically show electrocatalytic responses reminiscent of their dominant exposed surface facets in single crystal measurements. However, a majority of shape-controlled NPs are still very large compared to commercial catalyst NPs and therefore have sub-optimal mass activity. Additionally, the morphological stability has not been demonstrated sufficiently. For the possible application of such promising particles, it will be very interesting to see if the mass activity can be increased by decreasing the NP size, while retaining high NP stability

When NPs are used in electrocatalysis, it is of paramount importance that best practices are followed, with respect to immobilization, cleaning and characterization of the NPs on support electrodes. If these aspects are not properly considered, results obtained in different laboratories and experiments are difficult to compare. Additionally, when real catalysts are studied in model environments, this chapter has highlighted that it is essential to control mass transport and ohmic losses in order to understand the intrinsic behavior. Mass transport is also a very important consideration when studying model NP ensembles in model environments, particularly for reactions that have soluble intermediates that may re-adsorb on adjacent NPs, depending on the prevailing mass-transport rate and the inter-particle separation.

A major aspect of this chapter has been to highlight emerging frontier techniques that hold considerable promise for a breakthrough in understanding the fundamentals of NP electrocatalysis, through the study of individual NPs. This type of approach is particularly effective when the activity and structure can be determined and correlated at an individual NP. The main technical challenges are the spatial isolation of a

single NP and the measurement of the (often) very low electrochemical current generated at individual NPs. Three techniques were distinguished and discussed. First is the immobilization of individual particles on inert and ultrasmall probes, such as by electrodeposition. The use of this approach to study the ORR revealed how NP size influenced electrocatalytic activity and the outcome (products) of electrochemical processes.

The second approach is the discretized detection of individual NPs using UMEs. In this case the UME and NP couple are chosen such that the UME is inert to the turnover of a reactant in solution, but it occurs when a NP in solution is polarized upon landing on an UME surface. Several UME/NP combinations have been reported based on this approach, indicating that the approach is quite universal. Recently, this approach has been expanded by coupling to other techniques, such as electron microscopy, to allow the direct correlation between structure and activity on a single NP level. Improved quantification and analysis of NP landings are necessary for the further application of this technique, particularly the formulation of more advanced models for NP transport to the support electrode and the interaction of NPs with electrodes.

A final method for elucidating the electrochemistry of individual NPs is the application of probes with a high spatial resolution, such as scanning nanoelectrodes, scanning droplet cells, or advanced optical measurements, to screen two-dimensional NP ensembles. These measurements have shown heterogeneity in the activity of NPs of apparently similar size, suggesting that minute shape changes can significantly affect the catalytic activity of NPs.

Electrochemical measurements of NPs have now reached a critical phase, in which it has become possible to reveal catalytic activity of NPs from complex membrane electrode assemblies to individual NPs in model environments. The breadth of techniques and the information they provide will aid in the rational design of optimal catalysts for many reactions and greatly advance our understanding of electrochemical processes at the nanoscale.

Bibliography

[1] C. Q. Sun, B. K. Tay, X. T. Zeng, S. Li, T. P. Chen, J. Zhou, H. L. Bai and E. Y. Jiang, *J. Phys.: Condens. Matter*, 2002, **14**, 7781.

[2] D. Zanchet, H. Tolentino, M. M. Alves, O. Alves and D. Ugarte, *Chem. Phys. Lett.*, 2000, **323**, 167 – 172.

[3] A. N. Goldstein, C. M. Echer and A. P. Alivisatos, *Science*, 1992, **256**, 1425–1427.

[4] M. Haruta, *Chem. Rec.*, 2003, **3**, 75–87.

[5] M. T. M. Koper, *Nanoscale*, 2011, **3**, 2054–2073.

[6] Y. Li, E. Boone and M. A. El-Sayed, *Langmuir*, 2002, **18**, 4921–4925.

[7] S. Link and M. A. El-Sayed, *J. Phys. Chem. B*, 1999, **103**, 4212–4217.

[8] H.-B. Fu and J.-N. Yao, *J. Am. Chem. Soc.*, 2001, **123**, 1434–1439.

[9] B. Zhang, L. Fan, H. Zhong, Y. Liu and S. Chen, *J. Am. Chem. Soc.*, 2013, **135**, 10073–10080.

[10] J. J. Watkins and H. S. White, *Langmuir*, 2004, **20**, 5474–5483.

[11] C. P. Smith and H. S. White, *Anal. Chem.*, 1993, **65**, 3343–3353.

[12] R. He, S. Chen, F. Yang and B. Wu, *J. Phys. Chem. B*, 2006, **110**, 3262–3270.

[13] A. J. Bard, *J. Am. Chem. Soc.*, 2010, **132**, 7559–7567.

[14] A. J. Arvia, R. C. Salvarezza and W. E. Triaca, *J. New Mater. Electrochem. Syst.*, 2004, **7**, 133–143.

[15] F. Campbell and R. Compton, *Anal. Bioanal. Chem.*, 2010, **396**, 241–259.

[16] D. Hernández-Santos, M. B. González-García and A. C. García, *Electroanalysis*, 2002, **14**, 1225–1235.

[17] J. N. Anker, W. Paige Hall, O. Lyandres, N. C. Shah, J. Zhao and R. P. Van Duyne, *Nat. Mater.*, 2008, **7**, 442–453.

[18] S. Nie and S. R. Emory, *Science*, 1997, **275**, 1102–1106.

[19] K. Kneipp, H. Kneipp, I. Itzkan, R. R. Dasari and M. S. Feld, *Chem. Rev.*, 1999, **99**, 2957–2976.

[20] R. Kitsomboonloha, C. Ngambenjawong, W. Mohammed, M. B. Chaudhari, G. L. Hornyak and J. Dutta, *Micro Nano Lett.*, 2011, **6**, 342–344.

[21] Q. A. Pankhurst, J. Connolly, S. K. Jones and J. Dobson, *J. Phys. D: Appl. Phys.*, 2003, **36**, R167.

[22] S. M. Moghimi, A. C. Hunter and J. C. Murray, *Pharmacol. Rev.*, 2001, **53**, 283–318.

[23] B. D. Chithrani, A. A. Ghazani and W. C. W. Chan, *Nano Lett.*, 2006, **6**, 662–668.

[24] G. Wertheim, in *Small Particles and Inorganic Clusters*, ed. C. Chapon, M. Gillet and C. Henry, Springer Berlin Heidelberg, 1989, pp. 319–326.

[25] S. Proch, M. Wirth, H. S. White and S. L. Anderson, *J. Am. Chem. Soc.*, 2013, **135**, 3073–3086.

[26] G. Somorjai and J. Park, *Top. Catal.*, 2008, **49**, 126–135.

[27] G. Somorjai and Y. Li, *Introduction to Surface Chemistry and Catalysis*, Wiley & Sons, Hoboken, 2nd edn., 2010.

[28] J. K. Nørskov, T. Bligaard, J. Rossmeisl and C. H. Christensen, *Nat Chem*, 2009, **1**, 37–46.

[29] H. A. Gasteiger, S. S. Kocha, B. Sompalli and F. T. Wagner, *Appl. Catal., B*, 2005, **56**, 9–35.

[30] F. Maillard, S. Pronkin and E. Savinova, *A Surface Science Approach*, Wiley, Hoboken, 2009.

[31] R. W. Murray, *Chem. Rev.*, 2008, **108**, 2688–2720.

[32] S. M. Oja, M. Wood and B. Zhang, *Anal. Chem.*, 2013, **85**, 473–486.

[33] L. Rassaei, P. S. Singh and S. G. Lemay, *Anal. Chem.*, 2011, **83**, 3974–3980.

[34] H. Zhang, M. Jin and Y. Xia, *Angew. Chem., Int. Ed.*, 2012, **51**, 7656–7673.

[35] A. Chen and P. Holt-Hindle, *Chem. Rev.*, 2010, **110**, 3767–3804.

[36] M. Schulze, A. Schneider and E. Gülzow, *J. Power Sources*, 2004, **127**, 213 – 221.

[37] K. Mayrhofer, M. Arenz, B. Blizanac, V. Stamenkovic, P. Ross and N. Markovic, *Electrochim. Acta*, 2005, **50**, 5144 – 5154.

[38] S. Chen and A. Kucernak, *J. Phys. Chem. B*, 2003, **107**, 8392–8402.

[39] M. Debe, *Nature*, 2012, **486**, 43–51.

[40] G. Girishkumar, B. McCloskey, A. C. Luntz, S. Swanson and W. Wilcke, *J. Phys. Chem. Lett.*, 2010, **1**, 2193–2203.

[41] M. Armand and J. Tarascon, *Nature*, 2008, **451**, 652–657.

[42] V. R. Stamenkovic, B. Fowler, B. S. Mun, G. Wang, P. N. Ross, C. A. Lucas and N. M. Markovic, *Science*, 2007, **315**, 493–497.

[43] J. K. Nørskov, J. Rossmeisl, A. Logadottir, L. Lindqvist, J. R. Kitchin, T. Bligaard and H. Jónsson, *J. Phys. Chem. B*, 2004, **108**, 17886–17892.

[44] P. N. Markovic, N. M. Ross Jr, *Surf. Sci. Rep.*, 2002, **45**, 117–229.

[45] A. Kuzume, E. Herrero and J. M. Feliu, *J. Electroanal. Chem.*, 2007, **599**, 333–343.

[46] I. E. L. Stephens, A. S. Bondarenko, U. Gronbjerg, J. Rossmeisl and I. Chorkendorff, *Energy Environ. Sci.*, 2012, **5**, 6744–6762.

[47] M. Watanabe, H. Sei and P. Stonehart, *J. Electroanal. Chem. Interfac. Electrochem.*, 1989, **261**, 375–387.

[48] Y. E. Seidel, A. Schneider, Z. Jusys, B. Wickman, B. Kasemo and R. J. Behm, *Faraday Discuss.*, 2009, **140**, 167–184.

[49] S. Chen and A. Kucernak, *J. Phys. Chem. B*, 2004, **108**, 13984–13994.

[50] A. U. Nilekar, K. Sasaki, C. A. Farberow, R. R. Adzic and M. Mavrikakis, *J. Am. Chem. Soc.*, 2011, **133**, 18574–18576.

[51] S. M. M. Ehteshami and S. H. Chan, *Electrochim. Acta*, 2013, **93**, 334 – 345.

[52] N. Brandon, S. Skinner and B. Steele, *Annu. Rev. Mater. Res.*, 2003, **33**, 183–213.

[53] Y. Takasu, Y. Fujii, K. Yasuda, Y. Iwanaga and Y. Matsuda, *Electrochim. Acta*, 1989, **34**, 453 – 458.

[54] J. Meier, K. A. Friedrich and U. Stimming, *Faraday Discuss.*, 2002, **121**, 365–372.

[55] V. Rosca and M. T. M. Koper, *Electrochim. Acta*, 2008, **53**, 5199–5205.

[56] B. Alvarez-Ruiz, R. Gomez, J. M. Orts and J. M. Feliu, *J. Electrochem. Soc.*, 2002, **149**, D35–D45.

[57] B. E. Hayden, D. Pletcher and J.-P. Suchsland, *Angew. Chem., Int. Ed.*, 2007, **46**, 3530–3532.

[58] B. E. Hayden, D. Pletcher, J.-P. Suchsland and L. J. Williams, *Phys. Chem. Chem. Phys.*, 2009, **11**, 1564–1570.

[59] B. E. Hayden, D. Pletcher, J.-P. Suchsland and L. J. Williams, *Phys. Chem. Chem. Phys.*, 2009, **11**, 9141–9148.

[60] M. Haruta, *Catal. Today*, 1997, **36**, 153 – 166.

[61] C. T. Campbell, J. C. Sharp, Y. X. Yao, E. M. Karp and T. L. Silbaugh, *Faraday Discuss.*, 2011, **152**, 227–239.

[62] C. Galeano, R. Güttel, M. Paul, P. Arnal, A.-H. Lu and F. Schüth, *Chem. Eur. J.*, 2011, **17**, 8434–8439.

[63] A. S. K. Hashmi and G. J. Hutchings, *Angew. Chem., Int. Ed.*, 2006, **45**, 7896–7936.

[64] R. L. McCreery, *Chem. Rev.*, 2008, **108**, 2646–2687.

[65] L. M. Roen, C. H. Paik and T. D. Jarvi, *Electrochem. Solid-State Lett.*, 2004, **7**, A19–A22.

[66] P. Serp, M. Corrias and P. Kalck, *Appl. Catal., A*, 2003, **253**, 337 – 358.

[67] R. M. Crooks, M. Zhao, L. Sun, V. Chechik and L. K. Yeung, *Acc. Chem. Res.*, 2000, **34**, 181–190.

[68] G. R. Salazar-Banda, K. I. Eguiluz and L. A. Avaca, *Electrochem. Commun.*, 2007, **9**, 59 – 64.

[69] F. J. Vidal-Iglesias, J. Solla-Gullón, P. Rodríguez, E. Herrero, V. Montiel, J. M. Feliu and A. Aldaz, *Electrochem. Commun.*, 2004, **6**, 1080–1084.

[70] J. Solla-Gullón, P. Rodriguez, E. Herrero, A. Aldaz and J. M. Feliu, *Phys. Chem. Chem. Phys.*, 2008, **10**, 1359–1373.

[71] G. Sandmann, H. Dietz and W. Plieth, *J. Electroanal. Chem.*, 2000, **491**, 78–86.

[72] C. Granqvist and A. Hultåker, *Thin Solid Films*, 2002, **411**, 1 – 5.

[73] T. Minami, *Semicond. Sci. Technol.*, 2005, **20**, S35.

[74] R. M. Penner, *J. Phys. Chem. B*, 2002, **106**, 3339–3353.

[75] M. Bayati, J. M. Abad, R. J. Nichols and D. J. Schiffrin, *J. Phys. Chem. C*, 2010, **114**, 18439–18448.

[76] B. Scharifker and G. Hills, *Electrochim. Acta*, 1983, **28**, 879–889.

[77] J. V. Zoval, J. Lee, S. Gorer and R. M. Penner, *J. Phys. Chem. B*, 1998, **102**, 1166–1175.

[78] H. V. Patten, E. Ventosa, A. Colina, V. Ruiz, J. López-Palacios, A. J. Wain, S. C. Lai, J. V. Macpherson and P. R. Unwin, *J. Solid State Electrochem.*, 2011, **15**, 2331–2339.

[79] T. M. Day, P. R. Unwin and J. V. Macpherson, *Nano Lett.*, 2007, **7**, 51–57.

[80] T. M. Day, P. R. Unwin, N. R. Wilson and J. V. Macpherson, *J. Am. Chem. Soc.*, 2005, **127**, 10639–10647.

[81] B. M. Quinn, C. Dekker and S. G. Lemay, *J. Am. Chem. Soc.*, 2005, **127**, 6146–6147.

[82] B. Quinn and S. Lemay, *Adv. Mater.*, 2006, **18**, 855–859.

[83] C. C. Chen, C. S. C. Bose and K. Rajeshwar, *J. Electroanal. Chem.*, 1993, **350**, 161–176.

[84] M. T. Giacomini, E. A. Ticianelli, J. McBreen and M. Balasubramanian, *J. Electrochem. Soc.*, 2001, **148**, A323–A329.

[85] R. Schrebler, M. A. del Valle, H. Gómez, C. Veas and R. Córdova, *J. Electroanal. Chem.*, 1995, **380**, 219–227.

[86] J.-H. Ye and P. S. Fedkiw, *Electrochim. Acta*, 1996, **41**, 221–231.

[87] G. Kokkinidis, A. Papoutsis, D. Stoychev and A. Milchev, *J. Electroanal. Chem.*, 2000, **486**, 48–55.

[88] P. Sun, F. Li, C. Yang, T. Sun, I. Kady, B. Hunt and J. Zhuang, *J. Phys. Chem. C*, 2013, **117**, 6120–6125.

[89] H. Masuda, K. Yasui and K. Nishio, *Adv. Mater.*, 2000, **12**, 1031–1033.

[90] A. R. Howells, L. Hung, G. S. Chottiner and D. A. Scherson, *Solid State Ionics*, 2002, **150**, 53–62.

[91] K. L. Yeung and E. E. Wolf, *J. Vac. Sci. Technol., A*, 1992, **10**, 651–656.

[92] C. R. Henry, *Surf. Sci. Rep.*, 1998, **31**, 235–325.

[93] K. Yahikozawa, Y. Fujii, Y. Matsuda, K. Nishimura and Y. Takasu, *Electrochim. Acta*, 1991, **36**, 973–978.

[94] N. Tian, Z.-Y. Zhou, S.-G. Sun, Y. Ding and Z. L. Wang, *Science*, 2007, **316**, 732–735.

[95] J. Ustarroz, U. Gupta, A. Hubin, S. Bals and H. Terryn, *Electrochem. Commun.*, 2010, **12**, 1706–1709.

[96] J. Ustarroz, J. A. Hammons, T. Altantzis, A. Hubin, S. Bals and H. Terryn, *J. Am. Chem. Soc.*, 2013, **Accepted**.

[97] J. Ustarroz, X. Ke, A. Hubin, S. Bals and H. Terryn, *J. Phys. Chem. C*, 2012, **116**, 2322–2329.

[98] M. J. Williamson, R. M. Tromp, P. M. Vereecken, R. Hull and F. M. Ross, *Nat. Mater.*, 2003, **2**, 532–536.

[99] A. Radisic, P. M. Vereecken, J. B. Hannon, P. C. Searson and F. M. Ross, *Nano Lett.*, 2006, **6**, 238–242.

[100] J. Ustarroz, J. A. Hammons, Y. Van Ingelgem, M. Tzedaki, A. Hubin and H. Terryn, *Electrochem. Commun.*, 2011, **13**, 1320–1323.

[101] E. García-Pastoriza, J. Mostany and B. Scharifker, *J. Electroanal. Chem.*, 1998, **441**, 13 – 18.

[102] P. V. Dudin, P. R. Unwin and J. V. Macpherson, *J. Phys. Chem. C*, 2010, **114**, 13241–13248.

[103] P. L. Redmond, A. J. Hallock and L. E. Brus, *Nano Lett.*, 2005, **5**, 131–135.

[104] H. Liu and R. M. Penner, *J. Phys. Chem. B*, 2000, **104**, 9131–9139.

[105] H. Liu, F. Favier, K. Ng, M. P. Zach and R. M. Penner, *Electrochim. Acta*, 2001, **47**, 671–677.

[106] W. Plieth, H. Dietz, G. Sandmann, A. Meixner, M. Weber, P. Moyer and J. Schmidt, *Electrochim. Acta*, 1999, **44**, 3659–3666.

[107] M. Bayati, J. M. Abad, C. A. Bridges, M. J. Rosseinsky and D. J. Schiffrin, *J. Electroanal. Chem.*, 2008, **623**, 19–28.

[108] T. Brülle, A. Denisenko, H. Sternschulte and U. Stimming, *Phys. Chem. Chem. Phys.*, 2011, **13**, 12883–12891.

[109] T. Brülle, W. Ju, P. Niedermayr, A. Denisenko, O. Paschos, O. Schneider and U. Stimming, *Molecules*, 2011, **16**, 10059–10077.

[110] M. P. Zach and R. M. Penner, *Adv. Mater.*, 2000, **12**, 878–883.

[111] S. C. S. Lai, P. V. Dudin, J. V. Macpherson and P. R. Unwin, *J. Am. Chem. Soc.*, 2011, **133**, 10744–10747.

[112] J. L. Fransaer and R. M. Penner, *J. Phys. Chem. B*, 1999, **103**, 7643–7653.

[113] J. Dai and M. L. Bruening, *Nano Lett.*, 2002, **2**, 497–501.

[114] S. Joly, R. Kane, L. Radzilowski, T. Wang, A. Wu, R. E. Cohen, E. L. Thomas and M. F. Rubner, *Langmuir*, 2000, **16**, 1354–1359.

[115] S. Dante, Z. Hou, S. Risbud and P. Stroeve, *Langmuir*, 1999, **15**, 2176–2182.

[116] X. Shi, M. Shen and H. Möhwald, *Prog. Polym. Sci.*, 2004, **29**, 987 – 1019.

[117] X. Zhang and Z. Su, *Adv. Mater.*, 2012, **24**, 4574–4577.

[118] P. Bertoncello, M. Peruffo and P. R. Unwin, *Chem. Commun.*, 2007, 1597–1599.

[119] P. Allongue, M. Delamar, B. Desbat, O. Fagebaume, R. Hitmi, J. Pinson and J.-M. Savéant, *J. Am. Chem. Soc.*, 1997, **119**, 201–207.

[120] M. Delamar, R. Hitmi, J. Pinson and J. M. Saveant, *J. Am. Chem. Soc.*, 1992, **114**, 5883–5884.

[121] A. J. Downard, *Electroanalysis*, 2000, **12**, 1085–1096.

[122] J. Pinson and F. Podvorica, *Chem. Soc. Rev.*, 2005, **34**, 429–439.

[123] S. Mahouche-Chergui, S. Gam-Derouich, C. Mangeney and M. M. Chehimi, *Chem. Soc. Rev.*, 2011, **40**, 4143–4166.

[124] M. M. Waje, X. Wang, W. Z. Li and Y. S. Yan, *Nanotechnology*, 2005, **16**, S395–S400.

[125] D.-j. Guo and H.-l. Li, *Electrochem. Commun.*, 2004, **6**, 999–1003.

[126] D. J. Guo and H. L. Li, *Carbon*, 2005, **43**, 1259 – 1264.

[127] J. Turkevich, P. C. Stevenson and J. Hillier, *Discuss. Faraday Soc.*, 1951, **11**, 55–75.

[128] M. Brust, M. Walker, D. Bethell, D. J. Schiffrin and R. Whyman, *J. Chem. Soc., Chem. Commun.*, 1994, 801–802.

[129] B. L. Cushing, V. L. Kolesnichenko and C. J. O'Connor, *Chem. Rev.*, 2004, **104**, 3893–3946.

[130] R. Van Hardeveld and F. Hartog, *Surf. Sci.*, 1969, **15**, 189–230.

[131] Y. Xia, Y. Xiong, B. Lim and S. E. Skrabalak, *Angew. Chem., Int. Ed.*, 2009, **48**, 60–103.

[132] T. K. Sau and A. L. Rogach, *Adv. Mater.*, 2009, **22**, 1781–1804.

[133] K. Zhou and Y. Li, *Angew. Chem., Int. Ed.*, 2012, **51**, 602–613.

[134] Y. Niu and R. M. Crooks, *C. R. Chim.*, 2003, **6**, 1049–1059.

[135] F. Gröhn, B. J. Bauer, Y. A. Akpalu, C. L. Jackson and E. J. Amis, *Macromolecules*, 2000, **33**, 6042–6050.

[136] K. Esumi, A. Suzuki, A. Yamahira and K. Torigoe, *Langmuir*, 2000, **16**, 2604–2608.

[137] M. Zhao and R. M. Crooks, *Angew. Chem., Int. Ed.*, 1999, **38**, 364–366.

[138] R. M. Crooks and M. Zhao, *Adv. Mater.*, 1999, **11**, 217–220.

[139] M. Zhao, L. Sun and R. M. Crooks, *J. Am. Chem. Soc.*, 1998, **120**, 4877–4878.

[140] R. W. J. Scott, O. M. Wilson and R. M. Crooks, *J. Phys. Chem. B*, 2005, **109**, 692–704.

[141] F. Aulenta, W. Hayes and S. Rannard, *Eur. Polym. J.*, 2003, **39**, 1741 – 1771.

[142] F. Vögtle, G. Richardt and N. Werner, in *Functional Dendrimers*, Wiley-VCH Verlag GmbH & Co. KGaA, 2009, ch. 3, pp. 49–79.

[143] H. Ye and R. M. Crooks, *J. Am. Chem. Soc.*, 2005, **127**, 4930–4934.

[144] A. I. Yanson, P. Rodriguez, N. Garcia-Araez, R. V. Mom, F. D. Tichelaar and M. T. M. Koper, *Angew. Chem., Int. Ed.*, 2011, **50**, 6346–6350.

[145] P. Rodriguez, F. D. Tichelaar, M. T. M. Koper and A. I. Yanson, *J. Am. Chem. Soc.*, 2011, **133**, 17626–17629.

[146] A. I. Yanson, P. V. Antonov, P. Rodriguez and M. T. M. Koper, *Electrochim. Acta*, 2013, **In press**.

[147] A. I. Yanson, P. V. Antonov, Y. I. Yanson and M. T. M. Koper, *Electrochim. Acta*, 2013, **In press**.

[148] R. D. Deegan, O. Bakajin, T. F. Dupont, G. Huber, S. R. Nagel and T. A. Witten, *Nature*, 1997, **389**, 827–829.

[149] T. A. H. Nguyen, M. A. Hampton and A. V. Nguyen, *J. Phys. Chem. C*, 2013, **117**, 4707–4716.

[150] M. A. Hampton, T. A. Nguyen, A. V. Nguyen, Z. P. Xu, L. Huang and V. Rudolph, *J. Colloid Interface Sci.*, 2012, **377**, 456 – 462.

[151] R. G. Freeman, K. C. Grabar, K. J. Allison, R. M. Bright, J. A. Davis, A. P. Guthrie, M. B. Hommer, M. A. Jackson, P. C. Smith, D. G. Walter and M. J. Natan, *Science*, 1995, **267**, 1629–1632.

[152] W. Cheng, S. Dong and E. Wang, *Angew. Chem., Int. Ed.*, 2003, **42**, 449–452.

[153] W. Cheng, S. Dong and E. Wang, *J. Phys. Chem. B*, 2004, **108**, 19146–19154.

[154] Y. Li, J. T. Cox and B. Zhang, *J. Am. Chem. Soc.*, 2010, **132**, 3047–3054.

[155] T. Zhu, X. Fu, T. Mu, J. Wang and Z. Liu, *Langmuir*, 1999, **15**, 5197–5199.

[156] C. A. Goss, D. H. Charych and M. Majda, *Anal. Chem.*, 1991, **63**, 85–88.

[157] Y. Tang and W. Cheng, *Langmuir*, 2013, **29**, 3125–3132.

[158] K. C. Grabar, K. J. Allison, B. E. Baker, R. M. Bright, K. R. Brown, R. G. Freeman, A. P. Fox, C. D. Keating, M. D. Musick and M. J. Natan, *Langmuir*, 1996, **12**, 2353–2361.

[159] K. C. Grabar, P. C. Smith, M. D. Musick, J. A. Davis, D. G. Walter, M. A. Jackson, A. P. Guthrie and M. J. Natan, *J. Am. Chem. Soc.*, 1996, **118**, 1148–1153.

[160] W. Cheng, S. Dong and E. Wang, *Langmuir*, 2002, **18**, 9947–9952.

[161] S. L. Horswell, I. A. O'Nei and D. J. Schiffrin, *J. Phys. Chem. B*, 2003, **107**, 4844–4854.

[162] B. K. Jena, S. J. Percival and B. Zhang, *Anal. Chem.*, 2010, **82**, 6737–6743.

[163] D. Bethell, M. Brust, D. J. Schiffrin and C. Kiely, *J. Electroanal. Chem.*, 1996, **409**, 137–143.

[164] M. Brust, D. Bethell, C. J. Kiely and D. J. Schiffrin, *Langmuir*, 1998, **14**, 5425–5429.

[165] C. R. Bradbury, J. Zhao and D. J. Fermín, *J. Phys. Chem. C*, 2008, **112**, 10153–10160.

[166] J. Zhao, C. R. Bradbury and D. J. Fermín, *J. Phys. Chem. C*, 2008, **112**, 6832–6841.

[167] J. B. Shein, L. M. H. Lai, P. K. Eggers, M. N. Paddon-Row and J. J. Gooding, *Langmuir*, 2009, **25**, 11121–11128.

[168] J. Guo, C.-N. Ho and P. Sun, *Electroanal.*, 2011, **23**, 481–486.

[169] D. K. Schwartz, *Annu. Rev. Phys. Chem.*, 2001, **52**, 107–137.

[170] J. J. Gooding, F. Mearns, W. Yang and J. Liu, *Electroanalysis*, 2003, **15**, 81–96.

[171] A. Ulman, *Chem. Rev.*, 1996, **96**, 1533–1554.

[172] J. C. Love, L. A. Estroff, J. K. Kriebel, R. G. Nuzzo and G. M. Whitesides, *Chem. Rev.*, 2005, **105**, 1103–1170.

[173] F. Schreiber, *Prog. Surf. Sci.*, 2000, **65**, 151–257.

[174] G. Le Saux, S. Ciampi, K. Gaus and J. J. Gooding, *ACS Appl. Mater. Interfaces*, 2009, **1**, 2477–2483.

[175] M.-C. Chuang and J.-a. A. Ho, *RSC Advances*, 2012, **2**, 4092–4096.

[176] D. M. Adams, L. Brus, C. E. D. Chidsey, S. Creager, C. Creutz, C. R. Kagan, P. V. Kamat, M. Lieberman, S. Lindsay, R. A. Marcus, R. M. Metzger, M. E. Michel-Beyerle, J. R. Miller, M. D. Newton, D. R. Rolison, O. Sankey, K. S. Schanze, J. Yardley and X. Zhu, *J. Phys. Chem. B*, 2003, **107**, 6668–6697.

[177] A. Chou, P. K. Eggers, M. N. Paddon-Row and J. J. Gooding, *J. Phys. Chem. C*, 2009, **113**, 3203–3211.

[178] M. N. Paddon-Row, *Acc. Chem. Res.*, 1994, **27**, 18–25.

[179] D. J. Wold and C. D. Frisbie, *J. Am. Chem. Soc.*, 2001, **123**, 5549–5556.

[180] A. Barfidokht, S. Ciampi, E. Luais, N. Darwish and J. J. Gooding, *Anal. Chem.*, 2012, **85**, 1073–1080.

[181] W. Cheng, S. Dong and E. Wang, *Anal. Chem.*, 2002, **74**, 3599–3604.

[182] J. Zhao, M. Wasem, C. R. Bradbury and D. J. Fermín, *J. Phys. Chem. C*, 2008, **112**, 7284–7289.

[183] J. N. Chazalviel and P. Allongue, *J. Am. Chem. Soc.*, 2011, **133**, 762–4.

[184] J. N. Kuhn, C.-K. Tsung, W. Huang and G. A. Somorjai, *J. Catal.*, 2009, **265**, 209–215.

[185] J. Solla-Gullón, V. Montiel, A. Aldaz and J. Clavilier, *J. Electroanal. Chem.*, 2000, **491**, 69–77.

[186] H.-X. Zhang, H. Wang, Y.-S. Re and W.-B. Cai, *Chem. Commun.*, 2012, **48**, 8362–8364.

[187] J. Monzo, M. T. M. Koper and P. Rodriguez, *ChemPhysChem*, 2012, **13**, 709–715.

[188] F. J. Vidal-Iglesias, J. Solla-Gullón, E. Herrero, V. Montiel, A. Aldaz and J. M. Feliu, *Electrochem. Commun.*, 2011, **13**, 502–505.

[189] C. Aliaga, J. Y. Park, Y. Yamada, H. S. Lee, C.-K. Tsung, P. Yang and G. A. Somorjai, *J. Phys. Chem. C*, 2009, **113**, 6150–6155.

[190] J. Clavilier, R. Faure, G. Guinet and R. Durand, *J. Electroanal. Chem. Interfac. Electrochem.*, 1979, **107**, 205–209.

[191] J. Clavilier and D. Armand, *J. Electroanal. Chem. Interfac. Electrochem.*, 1986, **199**, 187–200.

[192] S. Trasatti and O. Petrii, *Pure Appl. Chem.*, 1991, **63**, 711–734.

[193] F. J. Vidal-Iglesias, R. M. Aran-Ais, J. Solla-Gullon, E. Herrero and J. M. Feliu, *ACS Catal.*, 2012, **2**, 901–910.

[194] J. Hernández, J. Solla-Gullón, E. Herrero, A. Aldaz and J. M. Feliu, *J. Phys. Chem. C*, 2007, **111**, 14078–14083.

[195] C. L. Green and A. Kucernak, *J. Phys. Chem. B*, 2002, **106**, 1036–1047.

[196] K. J. J. Mayrhofer, D. Strmcnik, B. B. Blizanac, V. Stamenkovic, M. Arenz and N. M. Markovic, *Electrochim. Acta*, 2008, **53**, 3181–3188.

[197] P. Ochal, J. L. G. de la Fuente, M. Tsypkin, F. Seland, S. Sunde, N. Muthuswamy, M. Rønning, D. Chen, S. Garcia, S. Alayoglu and B. Eichhorn, *J. Electroanal. Chem.*, 2011, **655**, 140 – 146.

[198] T. Vidaković, M. Christov and K. Sundmacher, *Electrochim. Acta*, 2007, **52**, 5606 – 5613.

[199] T. Housmans, J. Feliu and M. Koper, *J. Electroanal. Chem.*, 2004, **572**, 79 – 91.

[200] J. Grobelny, F. W. DelRio, N. Pradeep, D.-I. Kim, V. A. Hackley and R. F. Cook, in *Methods in Molecular Biology*, ed. J. Walker, Springer, Heidelberg, 2009, vol. 697, pp. 71–82.

[201] H. Borchert, E. V. Shevchenko, A. Robert, I. Mekis, A. Kornowski, G. Gruebel and H. Weller, *Langmuir*, 2005, **21**, 1931–1936.

[202] X. Liu, Q. Dai, L. Austin, J. Coutts, G. Knowles, J. Zou, H. Chen and Q. A. Huo, *J. Am. Chem. Soc.*, 2008, **130**, 2780–2782.

[203] V. Filipe, A. Hawe and W. Jiskoot, *Pharm. Res.*, 2010, **27**, 796–810.

[204] M. Kerker, *The Scattering of Light and other electromagnetic radiation*, Academic Press, London, 1969.

[205] V. Amendola, S. Polizzi and M. Meneghetti, *Langmuir*, 2007, **23**, 6766–6770.

[206] V. Amendola and M. Meneghetti, *J. Mater. Chem.*, 2007, **17**, 4705–4710.

[207] Z. L. Wang, *J. Phys. Chem. B*, 2000, **104**, 1153–1175.

[208] Y. E. Seidel, Z. Jusys, B. Wickman, B. Kasemo and R. J. Behm, *ECS Trans.*, 2010, **25**, 91–102.

[209] M. C. Henstridge and R. G. Compton, *Chem. Rec.*, 2012, **12**, 63–71.

[210] J. Guo and E. Lindner, *Anal. Chem.*, 2009, **81**, 130–138.

[211] N. C. Rudd, S. Cannan, E. Bitziou, I. Ciani, A. L. Whitworth and P. R. Unwin, *Anal. Chem*, 2005, **77**, 6205–6217.

[212] M. Gustavsson, H. Fredriksson, B. Kasemo, Z. Jusys, J. Kaiser, C. Jun and R. J. Behm, *J. Electroanal. Chem.*, 2004, **568**, 371–377.

[213] R. G. Compton and P. R. Unwin, *J. Electroanal. Chem. Interfac. Electrochem.*, 1986, **205**, 1 – 20.

[214] Y. E. Seidel, A. Schneider, Z. Jusys, B. Wickman, B. Kasemo and R. J. Behm, *Langmuir*, 2009, **26**, 3569–3578.

[215] I. Dumitrescu, D. F. Yancey and R. M. Crooks, *Lab Chip*, 2012, **12**, 986–993.

[216] I. Dumitrescu and R. M. Crooks, *Proc. Natl. Acad. Sci. U.S.A.*, 2012, **109**, 11493–11497.

[217] S. Amemiya, A. J. Bard, F.-R. F. Fan, M. V. Mirkin and P. R. Unwin, *Annu. Rev. Anal. Chem.*, 2008, **1**, 95–131.

[218] S. C. Lai, J. V. Macpherson and P. R. Unwin, *MRS Bull.*, 2012, **37**, 668–674.

[219] J. L. Fernández, D. A. Walsh and A. J. Bard, *J. Am. Chem. Soc.*, 2004, **127**, 357–365.

[220] S. Jayaraman and A. C. Hillier, *J. Phys. Chem. B*, 2003, **107**, 5221–5230.

[221] A. Minguzzi, M. A. Alpuche-Aviles, J. R. López, S. Rondinini and A. J. Bard, *Anal. Chem.*, 2008, **80**, 4055–4064.

[222] C. M. Sánchez-Sánchez and A. J. Bard, *Anal. Chem.*, 2009, **81**, 8094–8100.

[223] G. Lu, J. S. Cooper and P. J. McGinn, *J. Power Sources*, 2006, **161**, 106 – 114.

[224] M. V. Mirkin, W. Nogala, J. Velmurugan and Y. Wang, *Phys. Chem. Chem. Phys.*, 2011, **13**, 21196–21212.

[225] J. Zhang, R. M. Lahtinen, K. Kontturi, P. R. Unwin and D. J. Schiffrin, *Chem. Commun.*, 2001, 1818–1819.

[226] F. Li, I. Ciani, P. Bertoncello, P. R. Unwin, J. Zhao, C. R. Bradbury and D. J. Fermin, *J. Phys. Chem. C*, 2008, **112**, 9686–9694.

[227] B. E. Hayden, *Acc. Chem. Res.*, 2013.

[228] S. Guerin and B. E. Hayden, *J. Comb. Chem.*, 2006, **8**, 66–73.

[229] S. Guerin, B. E. Hayden, D. Pletcher, M. E. Rendall, J.-P. Suchsland and L. J. Williams, *J. Comb. Chem.*, 2006, **8**, 791–798.

[230] J. C. Meier, I. Katsounaros, C. Galeano, H. J. Bongard, A. A. Topalov, A. Kostka, A. Karschin, F. Schuth and K. J. J. Mayrhofer, *Energy Environ. Sci.*, 2012, **5**, 9319–9330.

[231] K. J. Mayrhofer, J. C. Meier, S. J. Ashton, G. K. Wiberg, F. Kraus, M. Hanzlik and M. Arenz, *Electrochem. Commun.*, 2008, **10**, 1144 – 1147.

[232] H. L. Xin, J. A. Mundy, Z. Liu, R. Cabezas, R. Hovden, L. F. Kourkoutis, J. Zhang, N. P. Subramanian, R. Makharia, F. T. Wagner and D. A. Muller, *Nano Lett.*, 2012, **12**, 490–497.

[233] Y. Yu, H. L. Xin, R. Hovden, D. Wang, E. D. Rus, J. A. Mundy, D. A. Muller and H. D. Abruña, *Nano Lett.*, 2012, **12**, 4417–4423.

[234] E. Endoh, S. Terazono, H. Widjaja and Y. Takimoto, *Electrochem. Solid-State Lett.*, 2004, **7**, A209–A211.

[235] A. Taniguchi, T. Akita, K. Yasuda and Y. Miyazaki, *J. Power Sources*, 2004, **130**, 42 – 49.

[236] T. S. Ahmadi, Z. L. Wang, T. C. Green, A. Henglein and M. A. El-Sayed, *Science*, 1996, **272**, 1924–1926.

[237] T. S. Ahmadi, Z. L. Wang, A. Henglein and M. A. El-Sayed, *Chem. Mater.*, 1996, **8**, 1161.

[238] M. Chen, B. Wu, J. Yang and N. Zheng, *Adv. Mater.*, 2012, **24**, 862–879.

[239] C. Burda, X. Chen, R. Narayanan and M. A. El-Sayed, *Chem. Rev.*, 2005, **105**, 1025–1102.

[240] R. Narayanan and M. A. El-Sayed, *J. Phys. Chem. B*, 2005, **109**, 12663–12676.

[241] M. Grzelczak, J. Perez-Juste, P. Mulvaney and L. M. Liz-Marzan, *Chem. Soc. Rev.*, 2008, **37**, 1783–1791.

[242] S. Guo and E. Wang, *Nano Today*, 2011, **6**, 240–264.

[243] A. R. Tao, S. Habas and P. D. Yang, *Small*, 2008, **4**, 310–325.

[244] Z. M. Peng and H. Yang, *Nano Today*, 2009, **4**, 143–164.

[245] F. J. Vidal-Iglesias, N. Garcia-Aráez, V. Montiel, J. M. Feliu and A. Aldaz, *Electrochem. Commun.*, 2003, **5**, 22–26.

[246] F. J. Vidal-Iglesias, R. M. Aran-Ais, J. Solla-Gullon, E. Garnier, E. Herrero, A. Aldaz and J. M. Feliu, *Phys. Chem. Chem. Phys.*, 2012, **14**, 10258–10265.

[247] V. Grozovski, J. Solla-Gullon, V. Climent, E. Herrero and J. M. Feliu, *J. Phys. Chem. C*, 2010, **114**, 13802–13812.

[248] C. Wang, H. Daimon, Y. Lee, J. Kim and S. Sun, *J. Am. Chem. Soc.*, 2007, **129**, 6974–6975.

[249] Y. Kang, M. Li, Y. Cai, M. Cargnello, R. E. Diaz, T. R. Gordon, N. L. Wieder, R. R. Adzic, R. J. Gorte, E. A. Stach and C. B. Murray, *J. Am. Chem. Soc.*, 2013, **135**, 2741–2747.

[250] L. Lu, G. Yin, Z. Wang and Y. Gao, *Electrochem. Commun.*, 2009, **11**, 1596–1598.

[251] C. Wang, H. Daimon, T. Onodera, T. Koda and S. Sun, *Angew. Chem., Int. Ed.*, 2008, **47**, 3588–3591.

[252] M. Rodríguez-López, J. Solla-Gullón, E. Herrero, P. Tuñón, J. M. Feliu, A. Aldaz and A. Carrasquillo, *J. Am. Chem. Soc.*, 2010, **132**, 2233–2242.

[253] C. M. Sánchez-Sánchez, F. J. Vidal-Iglesias, J. Solla-Gullón, V. Montiel, A. Aldaz, J. M. Feliu and E. Herrero, *Electrochim. Acta*, 2010, **55**, 8252–8257.

[254] V. Bansal, V. Li, A. P. O'Mullane and S. K. Bhargava, *CrystEngComm*, 2010, **12**, 4280–4286.

[255] M. Duca, P. Rodriguez, A. I. Yanson and M. T. M. Koper, *Top. Catal.*, 2013, **Accepted**.

[256] Z.-Y. Zhou, N. Tian, J.-T. Li, I. Broadwell and S.-G. Sun, *Chem. Soc. Rev.*, 2011, **40**, 4167–4185.

[257] Y. Ding, Y. Gao, Z. L. Wanga, N. Tian, Z. Y. Zhou and S. G. Sun, *Appl. Phys. Lett.*, 2007, **91**, 121901.

[258] Z.-Y. Zhou, Z.-Z. Huang, D.-J. Chen, Q. Wang, N. Tian and S.-G. Sun, *Angew. Chem., Int. Ed.*, 2010, **49**, 411–414.

[259] Y.-J. Deng, N. Tian, Z.-Y. Zhou, R. Huang, Z.-L. Liu, J. Xiao and S.-G. Sun, *Chem. Sci.*, 2012, **3**, 1157–1161.

[260] N. Tian, Z.-Y. Zhou, N.-F. Yu, L.-Y. Wang and S.-G. Sun, *J. Am. Chem. Soc.*, 2010, **132**, 7580–7581.

[261] Z.-Y. Zhou, S.-J. Shang, N. Tian, B.-H. Wu, N.-F. Zheng, B.-B. Xu, C. Chen, H.-H. Wang, D.-M. Xiang and S.-G. Sun, *Electrochem. Commun.*, 2012, **22**, 61–64.

[262] N. Tian, J. Xiao, Z.-Y. Zhou, H.-X. Liu, Y.-J. Deng, L. Huang, B.-B. Xu and S.-G. Sun, *Faraday Discuss.*, 2013, **162**, 77–89.

[263] Z. Y. Zhou, N. Tian, Z. Z. Huang, D. J. Chen and S. G. Sun, *Faraday Discuss.*, 2008, **140**, 81–92.

[264] N. Tian, Z.-Y. Zhou and S.-G. Sun, *Chem. Commun.*, 2009, **0**, 1502–1504.

[265] Q. Cheng, Y.-X. Jiang, N. Tian, Z.-Y. Zhou and S.-G. Sun, *Electrochim. Acta*, 2010, **55**, 8273–8279.

[266] Y.-X. Chen, S.-P. Chen, Z.-Y. Zhou, N. Tian, Y.-X. Jiang, S.-G. Sun, Y. Ding and Z. L. Wang, *J. Am. Chem. Soc.*, 2009, **131**, 10860.

[267] Q.-S. Chen, Z.-Y. Zhou, F. J. Vidal-Iglesias, J. Solla-Gullón, J. M. Feliu and S.-G. Sun, *J. Am. Chem. Soc.*, 2011, **133**, 12930–12933.

[268] H.-X. Liu, N. Tian, M. P. Brandon, J. Pei, Z.-C. Huangfu, C. Zhan, Z.-Y. Zhou, C. Hardacre, W.-F. Lin and S.-G. Sun, *Phys. Chem. Chem. Phys.*, 2012, **14**, 16415–16423.

[269] H.-X. Liu, N. Tian, M. P. Brandon, Z.-Y. Zhou, J.-L. Lin, C. Hardacre, W.-F. Lin and S.-G. Sun, *ACS Catal.*, 2012, **2**, 708–715.

[270] R. Huang, Y.-H. Wen, Z.-Z. Zhu and S.-G. Sun, *J. Mater. Chem.*, 2011, **21**, 11578–11584.

[271] Y. Wen, H. Fang, Z. Zhu and S. Sun, *Phys. Lett. A*, 2009, **373**, 272–276.

[272] Y.-H. Wen, H. Fang, Z.-Z. Zhu and S.-G. Sun, *Chem. Phys. Lett.*, 2009, **471**, 295–299.

[273] S. Cherevko, A. A. Topalov, I. Katsounaros and K. J. Mayrhofer, *Electrochem. Commun.*, 2013, **28**, 44 – 46.

[274] A. A. Topalov, I. Katsounaros, M. Auinger, S. Cherevko, J. C. Meier, S. O. Klemm and K. J. J. Mayrhofer, *Angew. Chem., Int. Ed.*, 2012, **51**, 12613–12615.

[275] J. T. Cox and B. Zhang, *Annual Review of Analytical Chemistry*, 2012, **5**, 253–272.

[276] C. J. Slevin, N. J. Gray, J. V. Macpherson, M. A. Webb and P. R. Unwin, *Electrochem. Commun.*, 1999, **1**, 282–288.

[277] J. L. Conyers and H. S. White, *Anal. Chem.*, 2000, **72**, 4441–4446.

[278] P. Sun and M. V. Mirkin, *Anal. Chem.*, 2006, **78**, 6526–6534.

[279] R. M. Penner, M. J. Heben, T. L. Longin and N. S. Lewis, *Science*, 1990, **250**, 1118–1121.

[280] G. P. Kittlesen, H. S. White and M. S. Wrighton, *J. Am. Chem. Soc.*, 1984, **106**, 7389–7396.

[281] O. Ordeig, C. E. Banks, T. J. Davies, J. del Campo, R. Mas, F. X. Munoz and R. G. Compton, *Analyst*, 2006, **131**, 440–445.

[282] S. E. F. Kleijn, A. I. Yanson and M. T. M. Koper, *J. Electroanal. Chem.*, 2012, **666**, 19–24.

[283] F. J. M. Hoeben, F. S. Meijer, C. Dekker, S. P. J. Albracht, H. A. Heering and S. G. Lemay, *ACS Nano*, 2008, **2**, 2497–2504.

[284] D. Krapf, M.-Y. Wu, R. M. M. Smeets, H. W. Zandbergen, C. Dekker and S. G. Lemay, *Nano Lett.*, 2005, **6**, 105–109.

[285] G. Mészáros, C. Li, I. Pobelov and T. . Wandlowski, *Nanotechnology*, 2007, **18**, 424004.

[286] G. Mészáros, S. Kronholz, S. Kartháuser, D. Mayer and T. Wandlowski, *Appl. Phys. A: Mater. Sci. Process.*, 2007, **87**, 569–575.

[287] N. Ebejer, M. Schnippering, A. W. Colburn, M. A. Edwards and P. R. Unwin, *Anal. Chem.*, 2010, **82**, 9141–9145.

[288] M. E. Snowden, A. G. Güell, S. C. S. Lai, K. McKelvey, N. Ebejer, M. A. O'Connell, A. W. Colburn and P. R. Unwin, *Anal. Chem.*, 2012, **84**, 2483–2491.

[289] A. G. Güell, N. Ebejer, M. E. Snowden, K. McKelvey, J. V. Macpherson and P. R. Unwin, *Proc. Natl. Acad. Sci. USA*, 2012.

[290] A. G. Güell, N. Ebejer, M. E. Snowden, J. V. Macpherson and P. R. Unwin, *J. Am. Chem. Soc.*, 2012, **134**, 7258–7261.

[291] S. C. S. Lai, A. N. Patel, K. McKelvey and P. R. Unwin, *Angew. Chem., Int. Ed.*, 2012, **51**, 5405–5408.

[292] H. V. Patten, S. C. S. Lai, J. V. Macpherson and P. R. Unwin, *Anal. Chem.*, 2012, **84**, 5427–5432.

[293] S. E. F. Kleijn, S. C. S. Lai, T. S. Miller, A. I. Yanson, M. T. M. Koper and P. R. Unwin, *J. Am. Chem. Soc.*, 2012, **134**, 18558–18561.

[294] A. N. Patel, K. McKelvey and P. R. Unwin, *J. Am. Chem. Soc.*, 2012, **134**, 20246–20249.

[295] A. N. Patel, M. G. Collignon, M. A. O'Connell, W. O. Y. Hung, K. McKelvey, J. V. Macpherson and P. R. Unwin, *J. Am. Chem. Soc.*, 2012, **134**, 20117–20130.

[296] B. D. B. Aaronson, C.-H. Chen, H. Li, M. T. M. Koper, S. C. S. Lai and P. R. Unwin, *J. Am. Chem. Soc.*, 2013, **135**, 3873–3880.

[297] N. Ebejer, A. G. Güell, S. C. Lai, K. McKelvey, M. E. Snowden and P. R. Unwin, *Annual Review of Analytical Chemistry*, 2013, **6**, 329–351.

[298] M. Lohrengel, A. Moehring and M. Pilaski, *Electrochim. Acta*, 2001, **47**, 137 – 141.

[299] C. G. Williams, M. A. Edwards, A. L. Colley, J. V. Macpherson and P. R. Unwin, *Anal. Chem.*, 2009, **81**, 2486–2495.

[300] T. Suter and H. Böhni, *Electrochim. Acta*, 1997, **42**, 3275 – 3280.

[301] J. W. Schultze, M. Pilaski, M. M. Lohrengel and U. Konig, *Faraday Discuss.*, 2002, **121**, 211–227.

[302] F. Cortes-Salazar, A. Lesch, D. Momotenko, J.-M. Busnel, G. Wittstock and H. H. Girault, *Anal. Methods*, 2010, **2**, 817–823.

[303] M. Carminati, G. Ferrari, D. Bianchi and M. Sampietro, *Electrochim. Acta*, 2013.

[304] J. J. Watkins, J. Chen, H. S. White, H. D. Abruña, E. Maisonhaute and C. Amatore, *Anal. Chem.*, 2003, **75**, 3962–3971.

[305] A. J. Bard and L. R. Faulkner, *Electrochemical Methods, Fundamentals and Applications*, John Wiley & Sons, New York, 2nd edn., 2001.

[306] X. Xiao and A. J. Bard, *J. Am. Chem. Soc.*, 2007, **129**, 9610.

[307] S. Chen and A. Kucernak, *Electrochem. Commun.*, 2002, **4**, 80–85.

[308] S. Chen and A. Kucernak, *J. Phys. Chem. B*, 2004, **108**, 3262–3276.

[309] R. Tel-Vered and A. J. Bard, *J. Phys. Chem. B*, 2006, **110**, 25279–25287.

[310] J. Lakbub, A. Pouliwe, A. Kamasah, C. Yang and P. Sun, *Electroanalysis*, 2011, **23**, 2270–2274.

[311] N. Nioradze, R. Chen, J. Kim, M. Shen, P. Santhosh and S. Amemiya, *Anal. Chem.*, 2013, **85**, 6198–6202.

[312] R. A. Lazenby, K. McKelvey and P. R. Unwin, *Anal. Chem.*, 2013, **85**, 2937–2944.

[313] W. Nogala, J. Velmurugan and M. V. Mirkin, *Anal. Chem.*, 2012, **84**, 5192–5197.

[314] K. McKelvey, B. P. Nadappuram, P. Actis, Y. Takahashi, Y. E. Korchev, T. Matsue, C. Robinson and P. R. Unwin, *Anal. Chem.*, 2013, **85**, 7519–7526.

[315] B. Zhang, J. Galusha, P. G. Shiozawa, G. Wang, A. J. Bergren, R. M. Jones, R. J. White, E. N. Ervin, C. C. Cauley and H. S. White, *Anal. Chem.*, 2007, **79**, 4778–4787.

[316] J. Meier, J. Schiotz, P. Liu, J. K. Nørskov and U. Stimming, *Chem. Phys. Lett.*, 2004, **390**, 440–444.

[317] General-Discussion, *Faraday Discuss.*, 2002, **121**, 97–127.

[318] M. Heyrovsky, J. Jirkovsky and M. Struplova-Bartackova, *Langmuir*, 1995, **11**, 4300–4308.

[319] M. Heyrovsky, J. Jirkovsky and M. Struplova-Bartackova, *Langmuir*, 1995, **11**, 4309–4312.

[320] M. Heyrovsky, J. Jirkovsky and B. R. Mueller, *Langmuir*, 1995, **11**, 4293–4299.

[321] M. Heyrovsky and J. Jirkovsky, *Langmuir*, 1995, **11**, 4288–4292.

[322] A. V. Korshunov and M. Heyrovský, *Electroanalysis*, 2006, **18**, 423–426.

[323] B. M. Quinn, P. G. van 't Ho and S. G. Lemay, *J. Am. Chem. Soc.*, 2004, **126**, 8360–8361.

[324] S. E. Fosdick, M. J. Anderson, E. G. Nettleton and R. M. Crooks, *J. Am. Chem. Soc.*, 2013, **135**, 5994–5997.

[325] X. Xiao, F.-R. F. Fan, J. Zhou and A. J. Bard, *J. Am. Chem. Soc.*, 2008, **130**, 16669–16677.

[326] X. Xiao, S. Pan, J. S. Jang, F.-R. F. Fan and A. J. Bard, *J. Phys. Chem. C*, 2009, **113**, 14978–14982.

[327] S. E. F. Kleijn, B. Serrano-Bou, A. I. Yanson and M. T. M. Koper, *Langmuir*, 2013, **29**, 2054–2064.

[328] R. Dasari, D. A. Robinson and K. J. Stevenson, *J. Am. Chem. Soc.*, 2013, **135**, 570–573.

[329] P. V. Dudin, P. R. Unwin and J. V. Macpherson, *Phys. Chem. Chem. Phys.*, 2011, **13**, 17146–17152.

[330] L. Aldous and R. G. Compton, *Phys. Chem. Chem. Phys.*, 2011, **13**, 5279–5287.

[331] M. M. Ardakani, M. Karimi, Z. M.M. and S. Mirdehghan, *Int. J. Electrochem. Sci.*, 2008, **3**, 246 – 258.

[332] H. R. Zare and N. Nasirizadeh, *Electroanalysis*, 2006, **18**, 507–512.

[333] J. Kunze, I. Burgess, R. Nichols, C. Buess-Herman and J. Lipkowski, *J. Electroanal. Chem.*, 2007, **599**, 147–159.

[334] G. A. Attard, J.-Y. Ye, P. Jenkins, F. J. Vidal-Iglesias, E. Herrero and S.-G. Sun, *J. Electroanal. Chem.*, 2013, **688**, 249 – 256.

[335] H. Zhou, F.-R. F. Fan and A. J. Bard, *J. Phys. Chem. Lett.*, 2010, **1**, 2671–2674.

[336] S. J. Kwon, F.-R. F. Fan and A. J. Bard, *J. Am. Chem. Soc.*, 2010, **132**, 13165–13167.

[337] S. J. Kwon and A. J. Bard, *J. Am. Chem. Soc.*, 2012, **134**, 7102–7108.

[338] Y.-G. Zhou, N. V. Rees and R. G. Compton, *Angew. Chem., Int. Ed.*, 2011, **50**, 4219–4221.

[339] N. V. Rees, Y.-G. Zhou and R. G. Compton, *ChemPhysChem*, 2011, **12**, 1645–1647.

[340] Y.-G. Zhou, N. V. Rees and R. G. Compton, *ChemPhysChem*, 2011, **12**, 2085–2087.

[341] Y.-G. Zhou, N. V. Rees and R. G. Compton, *Chem. Phys. Lett.*, 2011, **511**, 183–186.

[342] Y.-G. Zhou, N. V. Rees and R. G. Compton, *Chem. Phys. Lett.*, 2011, **514**, 291–293.

[343] E. J. E. Stuart, N. V. Rees and R. G. Compton, *Chem. Phys. Lett.*, 2012, **531**, 94–97.

[344] Y.-G. Zhou, N. V. Rees and R. G. Compton, *Chem. Commun.*, 2012, **48**, 2510–2512.

[345] H. Zhou, J. H. Park, F.-R. F. Fan and A. J. Bard, *J. Am. Chem. Soc.*, 2012, **134**, 13212–13215.

[346] N. V. Rees, Y.-G. Zhou and R. G. Compton, *Chem. Phys. Lett.*, 2012, **525-26**, 69–71.

[347] S. J. Kwon, H. Zhou, F.-R. F. Fan, V. Vorobyev, B. Zhang and A. J. Bard, *Phys. Chem. Chem. Phys.*, 2011, **13**, 5394–5402.

[348] E. O. Barnes and R. G. Compton, *J. Electroanal. Chem.*, 2013, **693**, 73–78.

[349] E. J. F. Dickinson, N. V. Rees and R. G. Compton, *Chem. Phys. Lett.*, 2012, **528**, 44–48.

[350] E. J. E. Stuart, Y.-G. Zhou, N. V. Rees and R. G. Compton, *RSC Advances*, 2012, **2**, 12702–12705.

[351] J. V. Macpherson, D. Wakerley, A. Guell, L. Hutton, T. Miller and A. Bard, *Chem. Commun.*, 2013.

[352] K. Huang, A. Anne, M. A. Bahri and C. Demaille, *ACS Nano*, 2013.

[353] X. Shan, I. Diez-Perez, L. Wang, P. Wiktor, Y. Gu, L. Zhang, W. Wang, J. Lu, S. Wang, Q. Gong, J. Li and N. Tao, *Nature Nano*, 2012, **7**, 668–672.

[354] X. Shan, X. Huang, K. J. Foley, P. Zhang, K. Chen, S. Wang and N. Tao, *Anal. Chem.*, 2009, **82**, 234–240.

[355] X. Shan, U. Patel, S. Wang, R. Iglesias and N. Tao, *Science*, 2010, **327**, 1363–1366.

[356] A. Kumar, F. Ciucci, A. N. Morozovska, S. V. Kalinin and S. Jesse, *Nat Chem*, 2011, **3**, 707–713.